The Astrophysical Journal, 636:932–951, 2006 January 10

INVESTIGATING DISK EVOLUTION: A HIGH SPATIAL RESOLUTION MID-INFRARED SURVEY OF T TAURI STARS

C. McCabe,[1,2,3] A. M. Ghez,[1,4] L. Prato,[1,3,5] G. Duchêne,[1,6] R. S. Fisher,[7] and C. Telesco[8]

Received 2005 March 24; accepted 2005 September 16

ABSTRACT

We present a high spatial resolution, 10–20 μm survey of 65 T Tauri binary stars in Taurus, Ophiuchus, and Corona Australis using the Keck 10 m telescopes. Designed to probe the inner $\sim$1 AU region of the circumstellar disks around the individual stellar components in these binary systems, this study increases the number of binaries with spatially resolved measurements at 10 μm by a factor of $\sim$5. Combined with resolved near-infrared photometry and spectroscopic accretion diagnostics, we find that $\sim$10% of stars with a mid-infrared excess do not appear to be accreting. In contrast to an actively accreting disk system, these passive disks have significantly lower near-infrared colors that are, in most cases, consistent with photospheric emission, suggesting the presence of an inner disk hole. In addition, there appears to be a spectral type/mass dependence associated with the presence of a passive disk, with all passive disks occurring around M-type stars. The presence of a passive disk does not appear to be related to the fact that these objects are in visual binary systems; the passive disk systems span the entire range of binary separations present in the sample, and a similar fraction of passive disks is observed in a sample of single stars. The possibility that the passive disks are caused by the presence of an as yet undetected companion at a small separation (0.3–3 AU) is possible for any individual system; however, it cannot account for the spectral type dependence of the passive disk sample as a whole. We propose that these passive disks represent a subset of T Tauri stars that are undergoing significant disk evolution. The fraction of observed passive disks and the observed spectral type dependence can both be explained by models of disk evolution that include disk photoevaporation from the central star.

Subject headings: binaries: close — circumstellar matter — planetary systems: protoplanetary disks — stars: pre–main-sequence

Online material: machine-readable tables

1. INTRODUCTION

A key component in the formation and evolution of a star and its surrounding planetary system is believed to be the existence and evolution of a circumstellar disk. Ample evidence for the prevalence of these disks has been found around the young, low-mass, T Tauri stars, including excess emission above the photosphere at infrared and longer wavelengths (e.g., Beckwith et al. 1990; Sargent & Beckwith 1991), strong hydrogen emission lines indicative of the accretion of disk gas onto the central star (e.g., Hartmann et al. 1994), and direct images that resolve the disks in thermal emission (e.g., Dutrey et al. 1998; Guilloteau et al. 1999) and scattered light (e.g., Burrows et al. 1996; Stapelfeldt et al. 1998). While the formation of these disks is a natural consequence of the star formation process, the details of how they evolve are poorly understood. The way in which the disk material dissipates has important ramifications not only for the characteristics of the central star (e.g., rotation rate) but also for the potential for planet formation. One particular challenge to existing theories of disk evolution is the empirical evidence for two different timescales in the inner region, which is probed by the infrared excess. The first is the timescale for this inner disk region to survive as an optically thick structure and is relatively long ($\sim 3 \times 10^6$ yr on average, but up to 1×10^7 yr for some objects; Haisch et al. 2001). In contrast, the second is the timescale for small dust grains to be removed from this region and appears to be significantly shorter ($\sim 10^5$ yr; Skrutskie et al. 1990; Skinner et al. 1991; Wolk & Walter 1996; Stassun et al. 2001). The short transition timescale has been a considerable problem for models of disk evolution (e.g., Kenyon et al. 1996; Armitage et al. 1999), which generally invoke processes that operate on the viscous timescale of the disk ($\sim 10^7$ yr). While theorists have recently begun to explore other physical processes that could give rise to such a rapid disk evolution (e.g., Clarke et al. 2001), the physical processes behind disk evolution and dispersion are still much debated.

A key step to constraining the physical mechanisms responsible for disk evolution is the detection of young stars with disks that are in the process of dispersing. A number of surveys have been conducted to search for these so-called transition objects, stars that have disk characteristics that are intermediate between those with clear evidence for disks and those with no disk material (Skrutskie et al. 1990; Skinner et al. 1991; Wolk & Walter 1996; Duvert et al. 2000; Stassun et al. 2001). Most of these surveys take advantage of the significant difference between the near- and mid-infrared excess emission (i.e., $K[2.2\ \mu\mathrm{m}] - N[10\ \mu\mathrm{m}]$ color) from systems with and without disks, in order to establish the evolutionary state of a system. However, most of this work has been

[1] Department of Physics and Astronomy, UCLA, Box 951547, Knudsen Hall, Los Angeles, CA 90095-1547; mccabe@jpl.nasa.gov, ghez@astro.ucla.edu, lprato@lowell.edu.

[2] Current address: NASA Jet Propulsion Laboratory, California Institute of Technology, MS 183-900, 4800 Oak Grove Drive, Pasadena, CA 91109-8099.

[3] Visiting Astronomer at the Infrared Telescope Facility, which is operated by the University of Hawaii under cooperative agreement NCC 5-538 with the National Aeronautics and Space Administration, Office of Space Science, Planetary Astronomy Program.

[4] Institute of Geophysics and Planetary Physics, University of California, 1156 High Street, Santa Cruz, CA 95064.

[5] Current address: Lowell Observatory, 1400 West Mars Hill Road, Flagstaff, AZ 86001.

[6] Current address: Laboratoire d'Astrophysique, Observatoire de Grenoble, Universite Joseph Fourier, BP 53, F-38041 Grenoble Cedex 9, France; gaspard.duchene@obs.ujf-grenoble.fr.

[7] Gemini Observatory, 670 North A'ohoku Place, Hilo, HI 96720; fisher@gemini.edu.

[8] Department of Astronomy, University of Florida, P.O. Box 112055, 211 Bryant Space Science Center, Gainesville, FL 32611; telesco@astro.ufl.edu.

done at low angular resolution, with the mid-infrared data primarily taken from *IRAS*, which has a beam size of 30″ at 12 μm. At the distance to the nearest sites of star formation ($d = 140$ pc), this corresponds to 4200 AU, within which most young stars are observed to have stellar companions (e.g., Ghez et al. 1993; Leinert et al. 1993; Simon et al. 1995). The confusion introduced by these unresolved companions is well illustrated by the case of V773 Tau, which is one of the two candidate evolved disks identified by Stassun et al. (2001), based on the lack of accretion and near-infrared excess and considerable excess at mid-infrared wavelengths and longer. V773 Tau is a quadruple system, with three stellar companions within 0.″3 of the primary. Duchêne et al. (2003) show that the excess seen in V773 Tau is actually from the recently discovered optically invisible, infrared-bright companion only 0.″24 away from V773 Tau A. These infrared companions (IRCs) occur with a frequency of $\sim$10% in the T Tauri population, a suspiciously similar frequency to the observed fraction of transition objects in low spatial resolution surveys for evolved systems. It is clear that in order to search for transition objects around T Tauri stars, high spatial resolution observations that resolve the individual components in these young multiple systems are required.

In this study we have targeted 65 binaries in the nearby star-forming regions of Taurus, Ophiuchus, and Corona Australis in order to resolve the mid-infrared emission for each individual component and search for the presence of transition objects. A comparison of disk properties between stars in binary systems and a sample of single stars taken from the literature allows us to distinguish between several possible effects, such as mass, and the presence of a companion. The sample of T Tauri binary stars is presented in § 2, and the observations and data reduction are discussed in § 3. The observed distribution of T Tauri stars in the $K - L$ versus $K - N$ color plane is discussed in § 4; we have discovered a sample of T Tauri stars that have mid-infrared evidence for disks but that do not appear to be actively accreting. These results are discussed in § 5 in light of disk evolution models.

2. THE SAMPLE

A sample of T Tauri binary stars was compiled from Reipurth & Zinnecker (1993), Ghez et al. (1993, 1997), Leinert et al. (1993), Simon et al. (1995), and Walter et al. (1988). All objects in the sample are observable from the Keck telescopes ($\delta > -40^\circ$), have Two Micron All Sky Survey (2MASS) colors consistent with a reddened T Tauri star (see Appendix A), and have separations between 0.″2 and 8″ (28–1120 AU). The lower separation bound is set by the diffraction limit at 10 μm and the upper bound by the largest separation detectable in all observations assuming that the primary is centered on the arrays. The sample is composed of binaries located within 140 pc, in the Taurus ($d = 140$ pc; Elias 1978), Ophiuchus ($d = 140$ pc; de Geus & Burton 1991), and Corona Australis ($d = 130$ pc; Marraco & Rydgren 1981) star-forming regions. Of the 70 possible targets, 65 were observed in this study and are listed in Table 1 by star-forming region and in order of increasing separation. LkHa 332/G1, LkHa 332/G2, HBC 412, HBC 360, and NTTS 160946−1851 were not observed because of insufficient time. The distribution of binary separations has a median value of 0.″75. As a result, half of the sample stars have separations smaller than the canonical disk size (100 AU; e.g., Shu et al. 1987), and all have separations larger than the dominant emission region of the disk at wavelengths shorter than 10 μm (<1 AU).

The majority (66%) of the observed systems have spatially resolved spectroscopic measurements available in the literature (see Table 4), with spectral types ranging from G2.5 to M7.5, and have a median type of M2.5. For these systems we define the primary star to be the one with the earliest spectral type, i.e., highest mass. For the stars that lack spectral type information, the component that is brightest at K band is assumed to be the primary.

Many of these systems also have spectroscopic measurements of Hα (6563 Å) or Brγ (2.166 μm) line emission for each individual component in the binary, allowing us to determine the accretion status of each star. Historically, Hα equivalent widths have been used to determine the presence of accretion. For the stars that have resolved Hα measurements, we employ the Martín (1998) Hα equivalent width limits, which take into account the spectral type dependence of intrinsic chromospheric Hα emission to determine whether a star is accreting or not. For K spectral types and earlier, if the EW of Hα is more than 5 Å, then the system is accreting material. For M0–M2 spectral types, the limit is 10 Å, and for M3 spectral types and later, it is 20 Å. The use of Brγ emission lines as an accretion diagnostic is more recent (e.g., Prato & Simon 1997; Muzerolle et al. 1998). It is likely that some chromospheric contamination occurs, but how much has not been determined. If there are no resolved Hα measurements but resolved Brγ measurements are available, the presence [EW(Brγ) > 0] or absence of a Brγ line is used to define the accretion status, independent of spectral type. For the stars in the sample with a measured accretion status, 78% of them have been defined through Hα line emission. Altogether, of the sample with line emission measurements, 64% are actively accreting (CTTSs) while 36% are not (WTTSs), or are accreting at too low a level to be detectable.

Near-infrared K[2.2 μm] and L[3.5 μm] band photometry for each component in the binary system is available in the literature for 48 of the binary stars in the sample (White & Ghez 2001; Prato et al. 2003; Woitas et al. 2001 and references therein). In contrast, only 11 of these systems have been previously resolved at 10 μm (Ghez et al. 1991, 1994a; Stanke & Zinnecker 2000; Girart et al. 2004; McCabe et al. 2003).

3. OBSERVATIONS AND DATA REDUCTION

We obtained 10 μm images of all of the 65 systems in Table 1 and 18 μm data of 26 of them at the Keck telescopes. Complementary near-infrared observations (2–4 μm) of 25 systems not previously resolved in the 3–4 μm region and of 21 additional systems in the target sample were made at the NASA Infrared Telescope Facility (IRTF). The goal was to obtain near-simultaneous K- and L-band observations of each star when possible. Combined with information available in the literature (see § 1), 57 of the 65 stars in the sample have resolved photometry in the 2–4 μm window. Here we describe the observations and method of data reduction for each data set. A log of all observations made can be found in Table 2, which lists the telescope, camera, and filters used for each observing run.

3.1. *Mid-Infrared*

3.1.1. *Observations*

High angular resolution mid-infrared observations were made at the Keck 10 m telescopes using two instruments: OSCIR, a visiting mid-infrared (8–25 μm) camera (Telesco et al. 2000), and the Long Wavelength Spectrometer (LWS; Jones & Puetter 1993), the facility mid-infrared imaging spectrograph. With OSCIR, which has a 128×128 Si:As blocked impurity band (BIB) array with a plate scale of 0.″062 ± 0.″001 pixel^{-1}, an orientation of 0.°05 ± 0.°38, and a corresponding field of view of 7.″9 × 7.″9, the stars were imaged using the N-band ($\lambda = 10.8$ μm, $\Delta\lambda = 5.15$ μm) and IHW18 ($\lambda = 18.1$ μm, $\Delta\lambda = 1.6$ μm) filters. With

TABLE 1

T Tauri Binary Sample

Object	Separation[a] (arcsec)	R.A. (J2000.0)	Decl. (J2000.0)	References
		Taurus		
IS Tau	0.22	04 33 36.8	+26 09 50	1, 2, 3
GG Tau A	0.25	04 32 30.3	+17 31 41	1, 2, 4
FS Tau	0.27	04 22 02.1	+26 57 32	2, 3
IW Tau	0.27	04 41 04.7	+24 51 06	2, 3
V410 Tau	0.29	04 18 31.1	+28 27 16	4
V927 Tau	0.30	04 31 23.8	+24 10 54	3
Haro 6-37	0.30/2.7	04 46 59.0	+17 02 38	2, 5
XZ Tau	0.30	04 31 40.0	+18 13 58	1, 2
GH Tau	0.31	04 33 06.1	+24 09 45	1, 2
GN Tau	0.31	04 39 20.8	+25 45 03	3, 4, 6
CZ Tau	0.33	04 18 31.6	+28 16 59	2
LkHa 332	0.33	04 42 07.7	+25 23 13	2
UZ Tau	0.34/3.78	04 32 42.9	+25 52 32	1, 2, 3, 4
V807 Tau	0.41	04 33 06.7	+24 09 56	1, 2, 3
LkCa 3	0.49	04 14 48.0	+27 52 35	1, 2
DD Tau	0.56	04 18 31.1	+28 16 30	1, 2
HBC 351	0.61	03 52 02.3	+24 39 51	2
Haro 6-28	0.66	04 35 55.9	+22 54 36	2, 3
VY Tau	0.66	04 39 17.4	+22 47 54	2, 3
FV Tau	0.72	04 26 53.6	+26 06 55	1, 2, 3, 5
T Tau	0.73	04 21 59.4	+19 32 06	1, 2
FV Tau/c	0.74	04 26 54.4	+26 06 52	2, 3
FQ Tau	0.79	04 19 12.8	+28 29 36	2
UY Aur	0.88	04 51 47.3	+30 47 14	1, 2
FX Tau	0.90	04 30 29.6	+24 26 46	1, 2, 3
LkCa 7	1.05	04 19 41.3	+27 49 39	2
RW Aur	1.42	05 07 49.6	+30 24 05	1, 2, 4, 5
GG Tau B	1.48	04 32 30.3	+17 31 31	2, 4
HBC 358/9	1.58/20.	04 03 49.2	+26 10 54	2
HBC 356/7	2.0	04 03 14.1	+25 53 00	7
HBC 411	2.04	04 35 41.2	+24 11 08	2, 3, 5
HK Tau	2.40	04 31 50.5	+24 24 19	2, 3, 5
IT Tau	2.48	04 33 54.7	+26 13 30	3, 5
DK Tau	2.53	04 30 44.3	+26 01 24	2, 3, 5
UX Tau	2.7/5.9	04 30 03.9	+18 13 49	2, 5
HN Tau	3.1	04 33 39.3	+17 51 53	2, 5
V710 Tau	3.24	04 31 57.6	+18 21 37	2, 5
J4872	3.5	04 25 17.6	+26 17 51	5
HV Tau	4.00	04 38 35.3	+26 10 39	2, 3, 5, 6
HBC 354/5	5.0	03 54 35.6	+25 37 12	7
		Ophiuchus		
SR 24	0.20/6.0	16 26 58.8	−24 45 37	3, 5, 8
NTTS 162218−2420	0.24	16 25 19.2	−24 26 52	1
NTTS 155913−2233	0.29	16 02 10.5	−22 41 28	1
SR 12	0.30	16 27 19.5	−24 41 40	3, 8
V853 Oph	0.40	16 28 45.3	−24 28 17	1, 3
ROXs 31	0.48	16 27 52.0	−24 40 48	3
WSB 11	0.50	16 21 57.3	−22 38 16	5
SR 9	0.59	16 27 40.3	−24 22 03	1
WSB 3	0.60	16 18 49.5	−26 32 53	5
Haro 1-4	0.72	16 25 10.5	−23 19 14	1, 5
DoAr 51	0.77	16 32 11.8	−24 40 19	8
NTTS 155203−2338	0.80	16 32 11.8	−24 40 19	1
WSB 18	1.1	16 24 59.7	−24 56 01	5
WSB 26	1.2	16 26 18.3	−25 20 55	5
ROX 15	1.2	16 26 42.7	−24 20 29	5
AS 205	1.32	16 11 31.4	−18 38 26	1, 5
WSB 19	1.5	16 25 01.9	−24 59 33	5
DoAr 24E	2.03	16 26 23.3	−24 20 58	1, 3, 5

TABLE 1—*Continued*

Object	Separation[a] (arcsec)	R.A. (J2000.0)	Decl. (J2000.0)	References
DoAr 26	2.3	16 26 34.8	−23 45 41	5
WSB 4	2.8	16 18 50.3	−26 10 08	5
ROX 43	4.8	16 31 20.0	−24 40 02	3, 5
WSB 28	5.1	16 26 20.9	−24 08 51	5
SR 21	6.7	16 27 10.2	−24 19 16	3, 5
Corona Australis				
S CrA	1.3	19 01 08.5	−36 57 20	5
HBC 679	4.5	19 02 22.4	−36 55 41	5

NOTE.—Units of right ascension are hours, minutes, and seconds, and units of declination are degrees, arcminutes, and arcseconds.

[a] Two numbers, separated by a slash, highlight a triple system.

REFERENCES.—(1) Ghez et al. 1993; (2) Leinert et al. 1993; (3) Simon et al. 1995; (4) Ghez et al. 1997; (5) Reipurth & Zinnecker 1993; (6) Simon et al. 1996; (7) Walter et al. 1988; (8) Ghez et al. 1994b.

LWS, a 128×128 Si:As array with a plate scale of $0\farcs081 \pm 0\farcs002$ pixel^{-1} and orientation of $-3\fdg6 \pm 1^\circ$ (McCabe et al. 2003), wide bandpass imaging was not possible. Observations were therefore made using the narrowband filters OCLI-O ($\lambda = 8.8$ μm, $\Delta\lambda = 0.85$ μm), OCLI-S ($\lambda = 12.5$ μm, $\Delta\lambda = 1.2$ μm), and the SiC filter ($\lambda = 11.8$ μm, $\Delta\lambda = 2.3$ μm) when it became available. LWS provides a $10\farcs24$ square field of view. The plate scale and orientation of both cameras were calibrated using observations of wide (>2″) binary systems.

Both instruments were used in chop-nod mode, switching between on-source and sky frames at an average rate of 4.5 Hz. The chopper amplitude was set to 8″–10″ such that the off-source beam lay outside the field of view of the array. The average on-source integration time was 2–3 minutes, and, for all observing runs, observations of target stars were interleaved with observations of photometric standards, which are listed in Table 5.

3.1.2. *Data Reduction*

Observations in the mid-infrared are background dominated, with contributions from both thermal emission from the sky and the telescope and dome structure. Accurate background subtraction is therefore critical and was achieved through double-differencing chop pairs at the two nod positions. This double difference was repeated for each chop-nod data set taken and the results co-added. Most of the binary stars observed had at least one component bright enough to be detected in the double-difference image. For these data sets, the background-subtracted nod sets were shifted and averaged using the centroid on the detected point source. For the fainter systems that were not detected in a single nod set, no relative position shifting between each of the chop-nod sets was done. In general, the difference between the final FWHM for the shifted and nonshifted frames is small; this is consistent with the small centroid shifts detected for the majority (87%) of stars observed that show rms shifts of $0\farcs02$ (<0.3 pixels). A small constant background offset was usually present in the averaged images. The median background was measured in a large annulus around the primary star (typically $4\farcs8$ in radius, but dependent on the binary separation) and subtracted from the image. The inner radius of the annulus was checked against the encircled flux of the star to ensure that the annuli chosen were not contaminated by stellar flux.

TABLE 2
OBSERVATION LOG

Date (UT)	Telescope	Instrument	Filters
Mid-Infrared			
1998 May 9–11	Keck II	OSCIR	*N*, IHW18
1998 May 14–15	Keck II	OSCIR	*N*, IHW18
1999 May 5–6	Keck II	OSCIR	*N*, IHW18
1999 Nov 17–20	Keck II	OSCIR	*N*, IHW18
2001 May 10–12	Keck I	LWS	8.9, 12.5, 18.7
2002 Nov 12–13	Keck I	LWS	SiC
Near-Infrared			
2001 Dec 1	IRTF	NSFCAM	*K*, *L*
2001 May 26–27	IRTF	NSFCAM	*K*, *L*

3.1.3. *Astrometric and Photometric Analysis*

The astrometric and photometric properties of each star in the binary system were found through fitting observed point-spread functions (PSFs) to the data, a method based on that used by McCabe et al. (2002). We employed a two-step approach. First, aperture photometry was done by placing a circular aperture on the centroid[9] of each star observed, providing initial estimates for the stellar position and flux ratio. These were then used to create a model image of the observations, using both a model Gaussian PSF of variable FWHM and a library of observed single-star PSFs from the same night as the target. This $3n$ parameter model for n stellar components (x and y stellar positions, relative scale of star to model PSF) was then fitted to the data using `amoeba`, a downhill simplex technique (Press et al. 1992). The fitting criterion, the minimization of the sum of the residuals $\Sigma(\text{data} - \text{model})^2$, was calculated within a 20 pixel radius circular aperture around each component. Given that the data are background limited, with the noise level being approximately the same for all pixels, this was equivalent to minimizing χ^2. The flux of each stellar component was then measured using a 20 pixel aperture on the

[9] On wide binaries, the centroid was calculated for both stars. For close binaries with large flux ratios, the centroid was calculated for the primary, whereas for the secondary the position of peak flux was used.

individual best-fit component model and compared to the flux from a photometric standard. The relative fluxes are both aperture and air mass corrected. This method provides photometry relative to the observed standards; the absolute calibration of the photometric standards used is described in Appendix B. The results presented in Table 3 are from the PSF fit that provided the smallest subtraction residuals; the measurement uncertainties for each parameter were estimated from the standard deviation of the fits from each PSF used. For systems in which two stars were detected, the separation, position angle (P.A.), and flux ratio of the binary are reported in Table 3. The corresponding uncertainties were derived from the measurement uncertainties combined with the uncertainties in the plate scale and orientation of the camera. If the night was photometric, the photometry of each component also appears in Table 3, along with the total combined photometry.

In a number of cases, only one star in the binary system was detected. If that source was unresolved, a model of a single PSF star was fitted to find the best matching parameters. Determining which component is emitting depends primarily on the separation of the binary and whether observations resolve the binary at other wavelengths on the same night. For example, consecutive images at 10 and 18 μm, where both components are seen at 10 μm, will clarify the source of an 18 μm detection of a single component. If the source of the emission cannot be distinguished as either the primary or secondary, the magnitude appears in the ninth column of Table 3 marked with an asterisk to indicate that the primary/secondary designation is lacking. If the source is extended, PSF fitting was done assuming that a binary is present. If the system contains blended point sources that were not accurately fitted through PSF fitting, aperture photometry of the total (unresolved) system is provided. This occurred in only one case (LkCa 3), for which resolved observations were available in another 10 μm filter.

3.1.4. *Filter Comparison*

Because of the changing availability of mid-infrared instrumentation and their associated filters at the Keck telescope during our observing runs, four filters were used to probe these systems in the 10 μm region, each with slightly different central wavelengths and bandpasses. The majority (89%) of the systems were observed using either the wide *N*-band ($\Delta\lambda \sim 5$ μm) or SiC filters ($\Delta\lambda = 2.3$ μm), which are centered on the amorphous Si emission feature. In contrast, 11% of the systems were observed using the narrowband 8.8 and 12.5 μm filters ($\Delta\lambda \sim 1$ μm), which are centered on the edge of the silicate feature. Since the Si feature varies in strength from object to object and in time (e.g., Hanner et al. 1998; Natta et al. 2000; Przygodda et al. 2003), it is necessary to check that no large, systematic bias was introduced by using the slightly different 8.8 μm, 12.5 μm, SiC, and *N*-band filters.

To do this, we used the spectra of 16 typical T Tauri stars presented in Przygodda et al. (2003). Our method for the absolute calibration of the filters (see Appendix B) was applied, using the relative flux spectra of Przygodda et al. (2003). We linearly interpolated over the $\sim$0.7 μm gap in the spectra at $\sim$9.3 μm. The relative integrated fluxes were then measured for each of these spectra, through each of the filters used. We found that the SiC filter magnitudes are, on average, 0.02 mag different from *N*-band photometry, and at most 0.1 mag different. The 8.8 μm filter is on average 0.1 mag different from *N*-band magnitudes but can be as much as 0.5 mag different. On the other hand, the 12.5 μm filter is on average 0.3 mag different and as much as 0.5 mag different; this filter is therefore not used in quantifying colors. Most of these discrepancies are on the order of the average measurement uncertainties in the data set (0.11 mag for *N* band, 0.12 mag for SiC band, and 0.1 mag for 8.8 μm data). We define the index [*N*] as the estimate of the 10 μm flux provided by the measured SiC, *N*-band, and 8.8 μm fluxes, in this order of preference in the case of multiple measurements (where the order of preference is of most used filter to least used filter). In the rest of the paper, we directly compare stars measured in these different filters.

3.2. *Near-Infrared*

3.2.1. *Observations*

K-band ($\lambda = 2.21$ μm, $\Delta\lambda = 0.39$ μm) and *L*-band ($\lambda = 3.5$ μm, $\Delta\lambda = 0.61$ μm) observations were made at the NASA IRTF 3 m telescope, using NSFCAM (Rayner et al. 1993; Shure et al. 1994), the facility 256×256 In:Sb near-infrared camera, on 2001 May 26–28 and 2001 Nov 28–Dec 1 (UT). Two observing modes were used depending on the required angular resolution. For binaries with separations greater than 1″, we used NSFCAM in direct-imaging mode, with a plate scale of $0\farcs150 \pm 0\farcs006$ pixel^{-1}, an orientation of $0\fdg5 \pm 1\fdg2$, and a field of view of $37\farcs9 \times 37\farcs9$. The targets were imaged in a box-4 dither pattern with a $\sim$19″ dither size. This pattern was repeated 2–4 times depending on the brightness of the stars, with exposure times varying from 0.5 to 20 s per dither position. For binaries with separations less than 1″, speckle imaging observations were obtained with a plate scale of $0\farcs053 \pm 0\farcs001$ pixel^{-1} (White & Ghez 2001), with NSFCAM running in *movieburst* mode, allowing a limited amount of data to be obtained at a high duty cycle with an integration time of 0.1 s. Three to four stacks of 400 such images were taken on each object, interleaved with similar observations of known single stars and blank sky for calibration. Photometric standards were observed in both filters throughout each night.

3.2.2. *Data Reduction*

Each direct imaging dither pattern was reduced in the following manner: Two dither positions, with the star placed in diametrically opposite corners, were subtracted from each other, removing the sky background and dark current components. This difference image was then corrected for different pixel gains using a flat field and corrected for bad pixels. The subtracted pairs for each star were then registered and added together, providing two final, averaged images, one with a positive image of the binary and one with a negative image. Photometry was done on both the positive and negative images with the same PSF fitting method used for the mid-infrared observations (see § 3.1.3 for details). The resulting photometry is the average of the two, with the uncertainty estimated from the range in the measurements.

For the speckle observations, each data cube of 400 images was reduced; sky and dark current levels were subtracted and the images were flat-fielded and bad pixel corrected. A power spectrum of each image was created and divided by the power spectrum of a star that is known to be single and pointlike. The fringe pattern in the power spectrum is a function of the binary star separation, P.A., and flux ratio. A two-dimensional model was fitted to the fringe pattern to measure these parameters (for details see Ghez et al. 1995). To resolve the 180° ambiguity on the P.A. and to obtain photometry of the combined system, the speckle stacks were also shifted and added (Ghez et al. 1998), yielding an average image of the binary system. The photometric results presented in § 4 combine the measured flux ratio of the two components (from the power spectrum analysis) with the photometry of the combined system to get magnitudes and fluxes for each individual component. The binary parameters (separation, flux ratio, P.A.) are from the power spectrum analysis of the final, averaged images. In all cases, quoted uncertainties are derived from the

TABLE 3

OBSERVATIONAL RESULTS

OBJECT	DATE (UT)	FILTER	SEPARATION (arcsec)	P.A. (deg)	FLUX RATIO	MAGNITUDE[a]		
						Primary	Secondary	Total[b]
				Taurus				
IS Tau	2002 Nov 12	SiC	...	...	...	...	...	5.02 ± 0.11
GG Tau A	1999 Nov 17	*N*	0.24 ± 0.01	347 ± 3	1.03 ± 0.04	5.03 ± 0.17	5.07 ± 0.13	4.30 ± 0.15
	1999 Nov 17	IHW18	...	...	...	...	...	2.67 ± 0.12
FS Tau	1999 Nov 17	*N*	...	...	...	...	...	4.19 ± 0.18
IW Tau	2001 Dec 01	*L*	0.30 ± 0.01	185 ± 1	1.67 ± 0.03	8.62 ± 0.02	9.18 ± 0.02	8.11 ± 0.02
	2002 Nov 13	SiC	...	...	...	...	...	8.10 ± 0.14
V410 Tau AC	2002 Nov 13	SiC	...	...	...	...	...	7.17 ± 0.13
V927 Tau	2001 Dec 01	*K*	0.26 ± 0.01	292 ± 1	1.64 ± 0.06	9.23 ± 0.02	9.76 ± 0.03	8.71 ± 0.02
	2001 Dec 01	*L*	0.29 ± 0.02	291 ± 2	2.37 ± 0.2	7.82 ± 0.13	8.76 ± 0.16	7.44 ± 0.15
	2002 Nov 12	SiC	...	...	...	...	...	8.04 ± 0.15
Haro 6-37 Aa–Ab	2002 Nov 13	SiC	0.30 ± 0.01	181 ± 3	1.50 ± 0.14	5.04 ± 0.14	5.47 ± 0.10	4.48 ± 0.13
Haro 6-37 AB	2002 Nov 13	SiC	2.61 ± 0.07	39 ± 1	1.19 ± 0.20	4.48 ± 0.13	4.68 ± 0.13	3.82 ± 0.15
XZ Tau	1999 Nov 17	*N*	...	...	...	...	...	2.17 ± 0.15
GH Tau	1999 Nov 17	*N*	0.30 ± 0.01	111 ± 2	1.45 ± 0.05	5.75 ± 0.12	6.15 ± 0.09	5.17 ± 0.11
	1999 Nov 17	IHW18	...	...	...	...	...	3.70 ± 0.11
GN Tau	2001 Dec 01	*L*	0.36 ± 0.01	126 ± 1	1.53 ± 0.03	8.26 ± 0.07	7.80 ± 0.07	7.25 ± 0.07
	1999 Nov 17	*N*	...	...	...	...	...	6.66 ± 0.17
CZ Tau	2001 Dec 01	*K*	0.33 ± 0.01	88 ± 2	5.58 ± 0.41	9.51 ± 0.02	11.38 ± 0.08	9.33 ± 0.03
	2001 Dec 01	*L*	0.33 ± 0.01	92 ± 2	1.71 ± 0.09	8.90 ± 0.08	9.49 ± 0.09	8.40 ± 0.09
	1999 Nov 16	*N*	...	...	...	...	...	3.79 ± 0.13
	1999 Nov 17	IHW18	...	...	...	...	...	6.06 ± 0.18
LkHa 332	1999 Nov 17	*N*	0.34 ± 0.01	210 ± 1.	1.76 ± 0.08	4.96 ± 0.14	5.57 ± 0.12	4.47 ± 0.14
	1999 Nov 17	IHW18	...	...	...	...	...	3.87 ± 0.12
UZ Tau W	2001 Dec 01	*L*	0.35 ± 0.01	4 ± 1	1.65 ± 0.06	7.68 ± 0.58	8.23 ± 0.59	7.16 ± 0.84
	1999 Nov 16	*N*	0.37 ± 0.01	3.7 ± 0.6	1.17 ± 0.07	6.43 ± 0.08	6.60 ± 0.08	5.76 ± 0.08
	1999 Nov 17	IHW18	0.37 ± 0.01	2.1 ± 0.9	1.33 ± 0.05	4.64 ± 0.10	4.94 ± 0.08	4.03 ± 0.1
UZ Tau EW	2001 Dec 1	*K*	3.5 ± 0.1	275 ± 1	1.81 ± 0.08	7.60 ± 0.1	8.24 ± 0.05	7.12 ± 0.09
	2001 Dec 1	*L*	3.5 ± 0.1	276 ± 1	2.51 ± 0.08	6.78 ± 0.17	7.78 ± 0.13	6.42 ± 0.17
	1999 Nov 16	*N*	3.52 ± 0.06	272.9 ± 0.4	8.02 ± 0.88	3.50 ± 0.09	5.76 ± 0.08	3.37 ± 0.09
	1999 Nov 17	IHW18	3.44 ± 0.06	273.0 ± 0.4	8.79 ± 1.2	2.28 ± 0.11	4.64 ± 0.10	2.16 ± 0.11
V807 Tau	1999 Nov 17	*N*	...	...	...	...	...	5.27 ± 0.18*
	1999 Nov 17	IHW18	...	...	...	...	...	4.04 ± 0.11*
LkCa 3	2001 Dec 01	*K*	0.47 ± 0.01	72 ± 1	1.18 ± 0.03	8.06 ± 0.03	8.24 ± 0.03	7.39 ± 0.03
	2001 Dec 01	*L*	0.47 ± 0.01	72 ± 1	1.17 ± 0.01	8.02 ± 0.03	8.19 ± 0.04	7.35 ± 0.03
	1999 Nov 17	*N*	...	...	...	...	...	7.52 ± 0.19[c]
	1999 Nov 17	IHW18	...	...	...	...	...	...
	2002 Nov 13	SiC	0.48 ± 0.02	76 ± 2	1.41 ± 0.06	7.72 ± 0.11	8.10 ± 0.09	7.14 ± 0.10
DD Tau	1999 Nov 17	*N*	0.54 ± 0.01	179 ± 2	1.75 ± 0.08	4.53 ± 0.06	5.13 ± 0.06	4.04 ± 0.06
HBC 351	2001 Dec 01	*K*	0.55 ± 0.01	314 ± 1	3.61 ± 0.39	9.20 ± 0.04	10.6 ± 0.1	8.94 ± 0.05
	2001 Dec 01	*L*	0.54 ± 0.02	315 ± 1	5.14 ± 0.06	...	...	...
	2002 Nov 13	SiC	...	...	...	...	...	...
Haro 6-28	2001 Dec 01	*L*	0.65 ± 0.01	247 ± 1	2.07 ± 0.08	8.81 ± 0.30	9.60 ± 0.32	8.38 ± 0.36
	1999 Nov 17	*N*	0.64 ± 0.01	246.5 ± 0.4	0.94 ± 0.04	7.38 ± 0.16	7.31 ± 0.18	6.59 ± 0.19
	1999 Nov 17	IHW18	0.68 ± 0.01	245.1 ± 0.6	0.79 ± 0.07	5.85 ± 0.07	5.58 ± 0.07	4.96 ± 0.07
VY Tau	2001 Dec 01	*L*	0.67 ± 0.01	318 ± 1	6.14 ± 0.27	8.47 ± 0.08	10.45 ± 0.11	8.31 ± 0.09
	1999 Nov 17	*N*	...	...	...	...	...	6.63 ± 0.16*
FV Tau	1999 Nov 17	*N*	0.71 ± 0.02	92.1 ± 0.8	2.2 ± 0.2	4.07 ± 0.17	4.92 ± 0.12	3.66 ± 0.17
	1999 Nov 17	IHW18	0.67 ± 0.03	112 ± 1	1.51 ± 0.06	3.07 ± 0.13	3.52 ± 0.11	2.52 ± 0.13
T Tau	1999 Nov 17	*N*	0.67 ± 0.01	181.2 ± 0.4	0.89 ± 0.02	1.54 ± 0.15	1.41 ± 0.16	0.72 ± 0.17
	1999 Nov 17	IHW18	0.67 ± 0.02	181.6 ± 0.8	0.87 ± 0.01	−1.48 ± 0.10	−1.63 ± 0.1	−2.31 ± 0.1
FV Tau/c	1999 Nov 17	*N*	0.67 ± 0.02	112 ± 1	0.74 ± 0.09	8.59 ± 0.14	8.26 ± 0.17	7.66 ± 0.17
	1999 Nov 17	IHW18	...	...	...	...	...	...
	2002 Nov 12	SiC	0.68 ± 0.02	115 ± 1	0.75 ± 0.04	6.27 ± 0.07	5.96 ± 0.10	5.36 ± 0.09
FQ Tau	2001 Dec 01	*K*	0.73 ± 0.01	67 ± 1	0.77 ± 0.08	10.15 ± 0.06	9.87 ± 0.05	9.25 ± 0.06
	2001 Dec 01	*L*	0.73 ± 0.01	67 ± 1	0.68 ± 0.04	9.54 ± 0.04	9.12 ± 0.03	8.56 ± 0.03
	1999 Nov 20	*N*	0.66 ± 0.01	70 ± 1	1.13 ± 0.04	7.42 ± 0.04	7.55 ± 0.09	6.73 ± 0.07
	2002 Nov 12	SiC	0.74 ± 0.02	66 ± 1	1.05 ± 0.02	7.18 ± 0.09	7.24 ± 0.10	6.46 ± 0.10
UY Aur	1999 Nov 16	*N*	0.88 ± 0.01	227.6 ± 0.4	2.07 ± 0.03	3.37 ± 0.1	4.16 ± 0.08	2.94 ± 0.10
	1999 Nov 16	IHW18	0.87 ± 0.01	227.7 ± 0.4	2.41 ± 0.02	1.28 ± 0.05	2.23 ± 0.04	0.90 ± 0.05
FX Tau	2001 Dec 01	*L*	0.85 ± 0.02	289 ± 1	2.63 ± 0.08	7.60 ± 0.05	8.65 ± 0.06	7.25 ± 0.05
	1999 Nov 18	*N*	0.87 ± 0.02	289.4 ± 0.4	2.75 ± 0.11	5.36 ± 0.11	6.46 ± 0.06	5.03 ± 0.10
	1999 Nov 18	IHW18	0.84 ± 0.02	290.5 ± 0.5	2.79 ± 0.33	4.01 ± 0.10	5.13 ± 0.03	3.68 ± 0.08

TABLE 3—*Continued*

Object	Date (UT)	Filter	Separation (arcsec)	P.A. (deg)	Flux Ratio	Magnitude[a]		
						Primary	Secondary	Total[b]
LkCa 7	2001 Dec 01	*K*	0.98 ± 0.02	25 ± 1	1.851 ± 0.05	8.66 ± 0.03	9.33 ± 0.04	8.19 ± 0.03
	2001 Dec 01	*L*	0.99 ± 0.02	25 ± 1	1.866 ± 0.02	8.62 ± 0.01	9.29 ± 0.02	8.15 ± 0.01
	1999 Nov 18	*N*	...	...	...	...	...	8.23 ± 0.12*
RW Aur	1999 Nov 16	*N*	1.42 ± 0.02	254.6 ± 0.4	13.63 ± 0.06	3.12 ± 0.09	5.96 ± 0.09	3.04 ± 0.09
	1999 Nov 16	IHW18	1.38 ± 0.02	254.7 ± 0.4	10.89 ± 0.46	1.62 ± 0.05	4.22 ± 0.06	1.53 ± 0.05
GG Tau B	1999 Nov 18	*N*	1.43 ± 0.02	133.2 ± 0.4	6.75 ± 0.25	6.72 ± 0.11	8.80 ± 0.11	6.57 ± 0.12
HBC 358 AB	2001 Dec 1	*K*	1.55 ± 0.06	226 ± 1	1.777 ± 0.003	9.80 ± 0.06	10.43 ± 0.06	9.32 ± 0.06
	2001 Dec 1	*L*	1.55 ± 0.06	224 ± 2	1.77 ± 0.16	9.79 ± 0.04	10.41 ± 0.14	9.30 ± 0.08
	2002 Nov 13	SiC	...	...	...	...	...	...
HBC 358/359	2001 Dec 1	*K*	20.1 ± 0.8	267 ± 1	1.31 ± 0.08	9.51 ± 0.03	9.80 ± 0.06	8.89 ± 0.04
	2001 Dec 1	*L*	20.1 ± 0.8	267 ± 1	1.18 ± 0.35	9.61 ± 0.32	9.79 ± 0.04	8.94 ± 0.21
HBC 356/357	2001 Dec 1	*K*	1.26 ± 0.05	5 ± 2	1.04 ± 0.01	10.72 ± 0.03	10.77 ± 0.03	9.99 ± 0.03
	2001 Dec 1	*L*	1.25 ± 0.05	4 ± 2	1.1 ± 0.1	10.86 ± 0.01	10.92 ± 0.1	10.14 ± 0.06
	2002 Nov 13	SiC	...	...	...	...	...	...
HBC 411	2001 Dec 1	*L*	2.08 ± 0.08	175 ± 1	5.99 ± 0.24	7.86 ± 0.01	9.80 ± 0.04	7.69 ± 0.01
	2002 Nov 13	SiC	2.02 ± 0.05	175 ± 1	10.22 ± 0.08	4.68 ± 0.12	7.21 ± 0.12	4.58 ± 0.13
HK Tau	2001 Dec 1	*L*	2.39 ± 0.1	168.1 ± 2.7	25.5 ± 2.4	8.08 ± 0.1	11.58 ± 0.16	8.04 ± 0.1[d]
	2002 Nov 13	SiC	2.23 ± 0.06	170 ± 1	30 ± 4	5.33 ± 0.07	9.03 ± 0.16	5.30 ± 0.07
IT Tau	2001 Dec 1	*L*	2.4 ± 0.1	225 ± 2	3.94 ± 0.06	7.67 ± 0.07	9.15 ± 0.05	7.42 ± 0.07
	2002 Nov 13	SiC	2.31 ± 0.06	224 ± 1	2.95 ± 0.01	5.31 ± 0.11	6.48 ± 0.11	4.99 ± 0.11
DK Tau	2002 Nov 13	SiC	2.27 ± 0.06	117 ± 1	8.53 ± 0.04	3.42 ± 0.14	5.75 ± 0.13	3.30 ± 0.15
UX Tau AB	2002 Nov 12	SiC	5.6 ± 0.1	268 ± 1	11.9 ± 1.8	5.62 ± 0.11	8.31 ± 0.12	5.53 ± 0.12
UX Tau AC	2002 Nov 12	SiC	2.50 ± 0.3	181 ± 5	59.7 ± 7.2	5.62 ± 0.11	10.06 ± 0.07	5.60 ± 0.12
HN Tau	2002 Nov 13	SiC	...	...	...	...	...	3.53 ± 0.13*
V710 Tau	2002 Nov 12	SiC	3.06 ± 0.08	178 ± 1	12.73 ± 0.11	5.44 ± 0.10	8.21 ± 0.10	5.36 ± 0.1
J4872	2001 Dec 1	*K*	3.4 ± 0.1	234 ± 1	1.78 ± 0.06	8.58 ± 0.03	9.20 ± 0.06	8.09 ± 0.04
	2001 Dec 1	*L*	3.4 ± 0.1	234 ± 1	1.75 ± 0.02	8.53 ± 0.07	9.14 ± 0.1	8.04 ± 0.08
	2002 Nov 12	SiC	...	...	...	...	...	...
HV Tau	2001 Dec 1	*K*	4.0 ± 0.2	43 ± 1	73.3 ± 8.3	7.86 ± 0.04	12.2 ± 0.1	7.84 ± 0.04
	2001 Dec 1	*L*	3.9 ± 0.2	43 ± 1	36.4 ± 1.8	7.66 ± 0.04	11.34 ± 0.04	7.62 ± 0.04
	2002 Nov 13	SiC	4.1 ± 0.1	43 ± 1	1.20 ± 0.01	7.59 ± 0.13	7.78 ± 0.14	6.93 ± 0.14
HBC 355/354	2001 Dec 1	*K*	6.3 ± 0.3	298 ± 1	2.18 ± 0.03	10.15 ± 0.01	10.99 ± 0.01	9.74 ± 0.01
	2001 Dec 1	*L*	6.2 ± 0.3	298 ± 1	2.22 ± 0.1	10.16 ± 0.07	11.03 ± 0.11	9.76 ± 0.09
	2002 Nov 13	SiC	...	...	...	...	...	...
Ophiuchus								
SR 24N	2001 May 26	*K*	0.112 ± 0.002	63 ± 2	1.523 ± 0.03	8.50 ± 0.01	8.96 ± 0.01	7.95 ± 0.01
	2001 May 26	*L*	0.12 ± 0.01	59 ± 6	1.887 ± 0.16	6.80 ± 0.04	7.49 ± 0.07	6.34 ± 0.05
SR 24NS	1999 May 04	*N*	5.08 ± 0.08	347.7 ± 0.4	0.95 ± 0.01	3.50 ± 0.12	3.45 ± 0.12	2.72 ± 0.13
	1999 May 04	IHW18	5.01 ± 0.08	347.5 ± 0.4	1.87 ± 0.05	1.87 ± 0.07	2.55 ± 0.05	1.41 ± 0.06
NTTS162218−2420	2001 May 26	*K*	0.19 ± 0.004	147 ± 2	1.25 ± 0.12	8.29 ± 0.06	8.53 ± 0.07	7.65 ± 0.07
	2001 May 26	*L*	0.201 ± 0.004	145 ± 1	1.40 ± 0.01	8.22 ± 0.01	8.58 ± 0.01	7.63 ± 0.01
	2001 May 10	8.8	...	...	...	...	...	7.32 ± 0.15
	2001 May 10	12.5	...	...	...	...	...	...
NTTS155913−2233	1999 May 05	*N*	...	...	...	...	...	6.94 ± 0.12*
SR 12	2001 May 26	*K*	0.228 ± 0.004	82 ± 1	1.292 ± 0.02	8.90 ± 0.01	9.18 ± 0.01	8.28 ± 0.01
	2001 May 26	*L*	0.237 ± 0.005	83 ± 1	1.50 ± 0.02	8.73 ± 0.06	9.17 ± 0.07	8.18 ± 0.07
	2001 May 11	8.8	...	...	...	...	...	...
V853 OPH	2001 May 26	*K*	0.34 ± 0.01	93 ± 1	3.55 ± 0.16	8.22 ± 0.02	9.60 ± 0.04	7.95 ± 0.02
	2001 May 26	*L*	0.33 ± 0.01	94 ± 1	3.91 ± 0.19	7.64 ± 0.03	9.12 ± 0.06	7.39 ± 0.04
	1999 May 04	IHW18	...	...	...	...	...	3.62 ± 0.05
	1999 May 04	*N*	0.26 ± 0.04	101 ± 4	3.9 ± 0.4	5.94 ± 0.09	7.42 ± 0.06	5.69 ± 0.09
ROXs 31	2001 May 26	*K*	0.38 ± 0.01	252 ± 1	1.31 ± 0.04	8.68 ± 0.02	8.97 ± 0.03	8.06 ± 0.02
	2001 May 26	*L*	0.38 ± 0.01	252 ± 1	1.65 ± 0.09	8.31 ± 0.03	8.85 ± 0.04	7.79 ± 0.03
	1999 May 05	*N*	...	...	...	...	...	...
WSB 11	2001 May 27	*K*	0.47 ± 0.01	317 ± 1	2.22 ± 0.06	10.39 ± 0.01	11.26 ± 0.02	9.99 ± 0.01
	1998 May 10	*N*	0.48 ± 0.01	314.9 ± 0.6	0.94 ± 0.10	...	...	...
	1999 May 04	*N*	0.48 ± 0.01	317 ± 1	1.09 ± 0.18	7.64 ± 0.06	7.74 ± 0.06	6.94 ± 0.06
	1999 May 04	IHW18	...	...	...	...	...	...
SR 9	2001 May 26	*K*	0.59 ± 0.01	353 ± 1	10.82 ± 0.16	7.18 ± 0.02	9.77 ± 0.03	7.08 ± 0.02
	2001 May 26	*L*	0.61 ± 0.02	353 ± 1	13.88 ± 0.55	6.56 ± 0.02	9.41 ± 0.06	6.48 ± 0.02
	1999 May 04	*N*	0.59 ± 0.02	356.8 ± 0.7	9.54 ± 0.9	4.37 ± 0.09	6.82 ± 0.11	4.26 ± 0.10

TABLE 3—*Continued*

Object	Date (UT)	Filter	Separation (arcsec)	P.A. (deg)	Flux Ratio	Magnitude[a]		
						Primary	Secondary	Total[b]
WSB 3	2001 May 27	*K*	0.59 ± 0.01	159 ± 1	2.36 ± 0.01	9.47 ± 0.01	10.40 ± 0.01	9.09 ± 0.01
	2001 May 27	*L*	0.60 ± 0.02	159 ± 1	4.42 ± 0.24	9.07 ± 0.04	10.68 ± 0.08	8.85 ± 0.05
	2001 May 10	8.8	...	...	...	...	...	...
Haro 1-4	2001 May 26	*K*	0.74 ± 0.01	30 ± 1	3.37 ± 0.07	7.58 ± 0.02	8.90 ± 0.03	7.30 ± 0.02
	2001 May 26	*L*	0.75 ± 0.01	30 ± 1	5.88 ± 0.02	6.83 ± 0.02	8.75 ± 0.02	6.66 ± 0.02
	2001 May 11	8.8	0.73 ± 0.02	27 ± 1	3.17 ± 0.5	...	...	...
	2001 May 11	12.5	0.74 ± 0.02	26 ± 1	3.14 ± 0.3	...	...	...
	1998 May 09	*N*	0.76 ± 0.02	27.2 ± 0.6	1.77 ± 0.06	...	...	...
	1998 May 09	IHW18	0.76 ± 0.01	28.8 ± 0.4	2.51 ± 0.03	...	...	...
DoAr 51	2001 May 27	*K*	0.75 ± 0.02	79 ± 1	9.72 ± 2.64	7.75 ± 0.07	10.22 ± 0.27	7.64 ± 0.09
	2001 May 27	*L*	0.72 ± 0.02	79 ± 2	3.41 ± 0.41	7.86 ± 0.14	9.19 ± 0.21	7.58 ± 0.17
	1998 May 10	*N*	0.79 ± 0.02	77.6 ± 0.4	0.51 ± 0.09	...	...	...
NTTS155203−2338[e]	2001 May 26	*K*	0.62 ± 0.03	231 ± 1	3.76 ± 0.06	7.21 ± 0.03	8.65 ± 0.05	6.95 ± 0.03
	2001 May 26	*L*	0.73 ± 0.03	233 ± 2	5.68 ± 0.5	6.69 ± 0.03	8.57 ± 0.08	6.51 ± 0.04
	2001 May 10	8.8	0.72 ± 0.02	232 ± 1	5.34 ± 0.23	7.10 ± 0.05	8.92 ± 0.02	6.92 ± 0.05
	2001 May 10	12.5	...	...	...	7.49 ± 0.11	...	7.49 ± 0.11
	1998 May 09	*N*	0.73 ± 0.02	233.5 ± 0.8	4.36 ± 0.6	...	...	...
WSB 18	2001 May 27	*K*	0.97 ± 0.11	80 ± 1	1.15 ± 0.3	10.2 ± 0.2	10.38 ± 0.08	9.53 ± 0.16
	2001 May 27	*L*	1.04 ± 0.05	83 ± 1	0.841 ± 0.08	9.94 ± 0.13	9.75 ± 0.03	9.09 ± 0.08
	2001 May 12	8.8	1.03 ± 0.03	85 ± 1	3.87 ± 0.09	9.21 ± 0.08	7.74 ± 0.1	7.49 ± 0.1
	2001 May 12	12.5	1.01 ± 0.03	77 ± 3	4.89 ± 0.23	8.86 ± 0.08	7.14 ± 0.08	6.94 ± 0.08
WSB 26	2001 May 27	*K*	1.09 ± 0.05	26 ± 2	1.24 ± 0.01	9.87 ± 0.09	10.10 ± 0.08	9.23 ± 0.09
	2001 May 27	*L*	1.10 ± 0.05	25 ± 1	1.31 ± 0.04	9.13 ± 0.03	9.42 ± 0.01	8.51 ± 0.02
	1999 May 04	*N*	1.14 ± 0.02	24.6 ± 0.4	0.41 ± 0.03	7.25 ± 0.11	6.28 ± 0.11	5.91 ± 0.12
	1998 May 11	*N*	1.12 ± 0.02	23.2 ± 0.7	3.78 ± 0.2	...	...	...
	1999 May 04	IHW18	...	...	...	...	...	...
ROX 15	2001 May 27	*K*	1.40 ± 0.06	69 ± 1	3.15 ± 0.05	8.22 ± 0.09	9.47 ± 0.07	7.92 ± 0.09
	2001 May 27	*L*	1.40 ± 0.06	69 ± 1	2.90 ± 0.1	7.39 ± 0.08	8.55 ± 0.04	7.07 ± 0.07
	1998 May 11	*N*	1.39 ± 0.02	67.6 ± 0.4	4.86 ± 0.4	...	...	...
	1999 May 05	*N*	1.45 ± 0.02	68.7 ± 0.4	3.97 ± 0.18	5.71 ± 0.05	7.21 ± 0.09	5.47 ± 0.06
	1999 May 05	IHW18	...	...	...	...	...	...
AS 205	2001 May 27	*K*	1.30 ± 0.07	214 ± 1	2.81 ± 0.06	5.95 ± 0.1	7.07 ± 0.13	5.62 ± 0.11
	2001 May 27	*L*	1.32 ± 0.05	213 ± 1	2.90 ± 0.23	4.9 ± 0.1	6.05 ± 0.02	4.58 ± 0.08
	2001 May 10	8.8	1.30 ± 0.03	210 ± 1	2.74 ± 0.02	2.46 ± 0.15	3.55 ± 0.15	2.12 ± 0.16
	2001 May 10	12.5	1.30 ± 0.03	210 ± 1	3.48 ± 0.07	1.47 ± 0.15	2.82 ± 0.14	1.19 ± 0.16
	1998 May 11	*N*	1.31 ± 0.04	212.1 ± 0.6	4.44 ± 0.5	...	...	...
WSB 19	2001 May 27	*K*	1.48 ± 0.06	262 ± 1	2.12 ± 0.1	9.84 ± 0.04	10.66 ± 0.09	9.42 ± 0.06
	2001 May 27	*L*	1.49 ± 0.06	262 ± 1	2.68 ± 0.03	9.13 ± 0.02	10.20 ± 0.04	8.79 ± 0.03
	1999 May 05	*N*	1.51 ± 0.02	263.2 ± 0.4	2.38 ± 0.06	5.72 ± 0.06	6.67 ± 0.08	5.34 ± 0.07
	1999 May 05	IHW18	...	...	...	3.83 ± 0.16	...	3.83 ± 0.16
DoAr 24E	2001 May 27	*K*	1.98 ± 0.08	150 ± 1	2.30 ± 0.5	7.13 ± 0.14	8.0 ± 0.1	6.73 ± 0.14
	2001 May 27	*L*	1.98 ± 0.08	150 ± 1	0.78 ± 0.03	6.42 ± 0.09	6.15 ± 0.14	5.52 ± 0.12
	1998 May 10	*N*	2.00 ± 0.03	149.6 ± 0.4	0.35 ± 0.004	...	...	...
	1998 May 10	IHW18	2.01 ± 0.03	149.9 ± 0.4	0.40 ± 0.004	...	...	...
DoAr 26[f]	2001 May 27	*K*	2.23 ± 0.09	131 ± 1	3.60 ± 0.14	9.1 ± 0.3	10.4 ± 0.2	8.81 ± 0.32
	2001 May 27	*L*	2.22 ± 0.09	132 ± 2	6.17 ± 0.01	8.28 ± 0.05	10.25 ± 0.06	8.12 ± 0.05
	1998 May 11	*N*	2.27 ± 0.04	130.6 ± 0.5	8.16 ± 0.9	...	...	...
	1999 May 05	*N*	2.29 ± 0.04	131.4 ± 0.4	5.87 ± 0.10	6.54 ± 0.06	8.46 ± 0.06	6.37 ± 0.06
	1999 May 05	IHW18	...	...	...	...	...	...
WSB 4	2001 May 27	*K*	2.78 ± 0.11	130 ± 1	0.611 ± 0.002	10.92 ± 0.12	10.38 ± 0.12	9.86 ± 0.13
	2001 May 27	*L*	2.77 ± 0.12	130 ± 1	0.394 ± 0.02	10.65 ± 0.12	9.64 ± 0.13	9.28 ± 0.14
	2001 May 12	8.8	...	...	...	...	...	8.18 ± 0.10*
	2001 May 12	12.5	...	...	...	...	...	8.18 ± 0.07*
ROX 43	2001 May 26	*K*	4.41 ± 0.18	12 ± 1	2.70 ± 0.03	6.66 ± 0.01	7.74 ± 0.02	6.32 ± 0.01
	2001 May 26	*L*	4.40 ± 0.18	12 ± 1	4.78 ± 0.06	5.51 ± 0.01	7.221 ± 0.001	5.31 ± 0.01
	2001 May 11	8.8	...	...	...	...	...	...
	2001 May 11	12.5	...	...	...	...	...	...
WSB 28	2001 May 27	*K*	5.00 ± 0.2	358 ± 2	10.67 ± 3.36	9.540 ± 0.004	12.08 ± 0.3	9.44 ± 0.03
	2001 May 27	*L*	5.0 ± 0.2	358 ± 1	9.18 ± 1.26	9.49 ± 0.13	11.89 ± 0.3	9.38 ± 0.16
	2001 May 12	8.8	4.9 ± 0.1	356 ± 1	1.24 ± 0.04	9.41 ± 0.11	9.64 ± 0.08	8.77 ± 0.10
SR 21	1998 May 11	*N*	7.67 ± 0.12	177.9 ± 0.4	10.84 ± 5.27	...	...	...
	1998 May 11	IHW18	7.85 ± 0.13	179.1 ± 0.4	3.43 ± 1.2	...	...	...

TABLE 3—*Continued*

Object	Date (UT)	Filter	Separation (arcsec)	P.A. (deg)	Flux Ratio	Magnitude[a]		
						Primary	Secondary	Total[b]
Corona Australis								
S CrA	2001 May 26	*K*	1.30 ± 0.05	150 ± 1	3.27 ± 0.1	6.04 ± 0.09	7.33 ± 0.13	5.75 ± 0.10
	2001 May 26	*L*	1.30 ± 0.05	150 ± 1	3.44 ± 0.1	4.62 ± 0.06	5.97 ± 0.03	4.34 ± 0.05
	2001 May 12	8.8	1.27 ± 0.03	148 ± 1	1.43 ± 0.01	3.51 ± 0.11	3.90 ± 0.11	2.93 ± 0.12
	2001 May 12	12.5	1.27 ± 0.03	148 ± 1	1.32 ± 0.01	2.88 ± 0.07	3.18 ± 0.07	2.27 ± 0.07
	1998 May 10	*N*	1.31 ± 0.02	149.3 ± 0.4	1.74 ± 0.05	...	...	...
	1998 May 10	IHW18	1.30 ± 0.02	149.1 ± 0.4	1.29 ± 0.02	...	...	...
	1999 May 05	*N*	1.32 ± 0.02	149.4 ± 0.4	2.51 ± 0.06	2.63 ± 0.07	3.63 ± 0.05	2.26 ± 0.07
	1999 May 05	IHW18	1.30 ± 0.04	149.2 ± 0.6	1.81 ± 0.06	1.11 ± 0.11	1.75 ± 0.15	0.63 ± 0.13
HBC 679	2001 May 26	*L*	4.33 ± 0.18	57 ± 1	4.76 ± 0.7	8.64 ± 0.02	10.34 ± 0.15	8.43 ± 0.04
	2001 May 10	8.8	...	...	...	...	...	...
	2001 May 10	12.5	...	...	...	...	...	...

Note.—Table 3 is also available in machine-readable form in the electronic edition of the *Astrophysical Journal*.

[a] For the filters used here, Vega has the following fluxes: 33.99 Jy for *N* band, 11.96 Jy for IHW18, 49.26 Jy for 8.8 μm, 28.24 Jy for SiC, 24.96 Jy for 12.5 μm. See Appendix B for more details on the absolute photometric calibration.

[b] Represents the magnitude of both primary and secondary combined, unless the value is followed by an asterisk. In this case, the observations reveal one point source and it is not clear which component the flux belongs to.

[c] Chopping errors provide unresolved flux only.

[d] Secondary marginally resolved in IRTF *L*-band observations causing large uncertainties in fluxes from PSF fitting; used *L*-band results from White & Ghez (2001) for final sample.

[e] A third object, situated 11.″1 from NTTS 155203−2338 A at a P.A. of 164.°4, was observed at *K* band (12.2 ± 0.2 mag) and *L* band (11.57 ± 0.01 mag). Given the preponderance of objects within 1′ of NTTS 155203−2338, this is likely to be a background object but has not been confirmed.

[f] A third object, located 16.″5 away from DoAr 26 A at a P.A. of 49.°3, was also detected, with $K = 11.6 \pm 0.2$ mag and $L = 11.6 \pm 0.8$ mag. It is not known whether this object is physically associated with DoAr 26 or not.

standard deviation of results from the individual stacks, combined with the uncertainties in plate scale and orientation of the camera.

4. RESULTS

Measurements that produce flux ratios and/or absolute photometric results are presented in Table 3. In general, objects with $[N]$-band flux densities greater than 10 mJy and 18 μm fluxes greater than 30 mJy are clearly detected. We therefore took these values as upper limits in cases where no source was detected. Absolute photometry was obtained from our observations for 75, 93, 89, and 24 individual components at K, L, $[N]$, and 18 μm, respectively. Relative flux measurements for systems observed during nonphotometric conditions were made for one, four, and three systems at L, $[N]$, and 18 μm, respectively. There are nine systems (HBC 351, HBC 358, HBC 356, HBC 355, SR 12, ROXs 31, WSB 3, ROX 43, HBC 679) in which no stars were detected in the 8–13 μm window, and six (LkCa 3, FV Tau/c, WSB 11, WSB 26, ROX 15, DoAr 26) in which nothing was detected at 18 μm. No new components were identified in the mid-infrared that were not already identified at some other wavelength. Approximately 25% of the binary systems have inverted flux ratios at wavelengths longer than 2 μm; the brightest component at 2 μm is not necessarily the brightest at either 3.5 or 10 μm, highlighting the potential pitfalls in assigning long-wavelength, low spatial resolution measurements to the component that dominates at shorter wavelengths. These results increase the number of systems with spatially resolved measurements at 10 μm by a factor of $\sim$5.

We construct a final sample of 71 components in 35 systems that have high spatial resolution K-, L-, and $[N]$-band measurements; these are listed in Table 4. All but 4 of these 35 systems also have spatially resolved spectroscopic information, providing spectral type and accretion diagnostics for each stellar component. Measurements used in this final sample are first taken from our results and then supplemented with other work. Specifically, we have added two measurements from the literature at mid-infrared wavelengths (DoAr 24E and HK Tau, from Stanke & Zinnecker 2000; McCabe et al. 2003) and approximately half of the measurements at near-infrared wavelengths (see Table 4 for references).

For our final sample, dereddened $K - L$ versus $K - [N]$ and $K - [N]$ versus $[N] - 18$ colors are presented in Figure 1, with the symbol type representing whether or not the star is actively accreting. The dereddened colors for each component are also listed in Table 4, along with the visual extinction for the system (inferred using a method detailed in Appendix A), the spectral type when known, the spectroscopic accretion measure used (i.e., Hα or Brγ), and the EW of Hα emission when applicable. In both the $K - [N]$ and $[N] - 18$ color indices the stars are well separated into the three groups originally identified by Lada (1987), corresponding to photospheric emission (class III), disk emission (class II), and embedded protostellar emission (class I). Here we adopt the following mid-infrared color limits to delineate these groups:

1. Class I: $K - [N] > 4.5$.
2. Class II: $1.75 < K - [N] < 4.5$.
3. Class III: $K - [N] < 1$.

These correspond to the Wilking et al. (2001) spectral index limits, with three modifications: we include the flat spectrum class defined by Wilking et al. (2001) in our class I definition, we use a class II lower limit of $K - [N] = 1.75$ rather than $K - [N] = 2$, and we adopt a class III cutoff that is intermediate between those suggested by Wilking et al. (2001; $K - N = 2$) and Kenyon & Hartmann (1995; $K - [N] \sim 0.5$). The class III color limit therefore incorporates the photospheric contribution from even the lowest mass star in our sample.

Within our sample, we have detected three class I sources, 58 class II sources, and 10 class III sources. Since our sample was selected for T Tauri stars, we did not expect to detect many class I stars. All three class I stars (T Tau B, FV Tau/c B, and DoAr 24E B) are secondaries to class II primaries and are previously identified IRCs or high-accretion stars (Koresko et al. 1997; White &

TABLE 4

STELLAR COMPONENT COLORS

OBJECT	COMPONENT	A_v[a]	SPECTRAL TYPE	DEREDDENED		REFERENCES[b]		LINE?	EW(Hα) (Å)	T TAURI		REFERENCES	NOTES
				$K-L$	$K-[N]$	Mid-IR	Near-IR			Class	Type		
GG Tau	Aa	0.75	K7	0.79 ± 0.15	2.64 ± 0.17	1	3.2	Hα	42	II	C	5	
	Ab	...	M0.5	0.73 ± 0.16	3.42 ± 0.14	1	3.2	Hα	21	II	C	5	
Haro 6-37	B	3.89	M1	0.58 ± 0.08	3.76 ± 0.15	1	2	Hα	184	II	C	2	
GH Tau	A	1.04	M2	0.64 ± 0.25	2.83 ± 0.26	1	2	Hα	10	II	C	5	
	B	...	M2	0.81 ± 0.23	2.23 ± 0.23	1	2	Hα	10	II	C	5	
LkHa 332	A	3.58	K7	0.87 ± 0.10	3.06 ± 0.17	1	3.2	Hα	10.9	II	C	5	
	B	...	M2.5	−0.16 ± 0.14	3.29 ± 0.16	1	3.2	Hα	6.2	II	W	5	Passive
UZ Tau E	Aa–Ab	7.13	M1	0.44 ± 0.2	3.67 ± 0.13	1	1	Hα	74.	II	C	2	
UZ Tau W	A	0.28	M2	1.00 ± 0.60	2.25 ± 0.15	1	2.1	Hα	54.	II	C	5	
	B	...	M3	1.05 ± 0.61	2.68 ± 0.18	1	2.1	Hα	97.	II	C	5	
DD Tau	A	1.61	M3	1.16 ± 0.25	3.79 ± 0.14	1	2	Hα	206	II	C	5	
	B	...	M3	1.05 ± 0.29	3.66 ± 0.20	1	2	Hα	635.	II	C	5	
Haro 6-28	A	3.09	M2	0.82 ± 0.30	2.23 ± 0.17	1	3.1	Hα	57	II	C	5	
	B	...	M3.5	0.53 ± 0.32	2.80 ± 0.19	1	3.1	Hα	124	II	C	5	
FV Tau	A	6.68	K5	0.27 ± 0.21	3.47 ± 0.19	1	3.2	Hα	15.	II	C	5	
	B	...	K6	0.95 ± 0.22	3.01 ± 0.17	1	3.2	Hα	63.	II	C	5	
T Tau	A	[0.0]	K1	1.05 ± 0.32	3.84 ± 0.30	1	2	Hα	60	II	C	2	
	Ba–Bb	...	...	3.21 ± 0.32	5.78 ± 0.31	1	2	...	...	I	C	2	IRC
FV Tau/c	A	5.23	M2.5	0.17 ± 0.05	2.29 ± 0.08	1	3.2	Hα	17	II	W	2, 5	Passive
	B	...	M3.5	1.81 ± 0.08	5.40 ± 0.10	1	3.2	Hα	224	I	C	2, 5	IRC
FQ Tau	A	0.35	M3	0.59 ± 0.07	2.95 ± 0.11	1	1	Hα	110	II	C	5	
	B	...	M3.5	0.73 ± 0.06	2.61 ± 0.11	1	1	Hα	23	II	W[c]	5	Passive
UY Aur	A	2.05	K7	0.94 ± 0.06	4.16 ± 0.10	1	2	Hα	36.	II	C	5	
	B	...	M2	0.89 ± 0.07	4.13 ± 0.10	1	2	Hα	59.	II	C	5	
FX Tau	A	2.24	M1	0.87 ± 0.15	3.09 ± 0.18	1	2.1	Hα	13	II	C	5	
	B	...	M4	0.55 ± 0.17	2.72 ± 0.17	1	2.1	Hα	1	II	W	5	Passive
RW Aur	A	[0.0]	K1	1.11 ± 0.22	3.93 ± 0.22	1	3.2	Hα	76	II	C	2	
	B	...	K5	0.73 ± 0.25	2.69 ± 0.25	1	3.2	Hα	43.	II	C	2	
GG Tau	Ba	[0.0]	M6	0.81 ± 0.04	3.39 ± 0.11	1	2	Hα	21	II	C	2	
	Bb	...	M7.5	0.79 ± 0.17	3.22 ± 0.13	1	2	Hα	32.	II	C	2	
HK Tau	A	3.41	M1	0.64 ± 0.04	3.14 ± 0.08	10	2	Hα	50.	II	C	4	
	B	...	M2	0.28 ± 0.12	2.77 ± 0.17	10	2	Hα	12.5	II	C	4	
IT Tau	A	1.87	K3	0.24 ± 0.09	2.59 ± 0.12	1	2.1	Hα	21.7	II	C	4	
	B	...	M4	0.77 ± 0.13	3.42 ± 0.16	1	2.1	Hα	147.	II	C	4	
DK Tau	A	0.35	K9	0.97 ± 0.04	3.99 ± 0.14	1	2	Hα	31	II	C	4	
	B	...	M1	1.02 ± 0.08	3.22 ± 0.15	1	2	Hα	118.	II	C	4	
UX Tau	A	[0.0]	K5	0.76 ± 0.06	1.88 ± 0.12	1	2	Hα	9.5	II	C	2	
	B	...	M2	0.09 ± 0.06	0.67 ± 0.13	1	2	Hα	4.5	III	W	2	
	C	...	M5	0.38 ± 0.12	0.51 ± 0.11	1	2	Hα	8.5	III	W	2	
V710 Tau	A	[0.0]	M0.5	0.44 ± 0.04	3.32 ± 0.11	1	2	Hα	69	II	C	2	
	B	...	M2.5	0.31 ± 0.04	0.29 ± 0.11	1	2	Hα	7.2	III	W	2	
HV Tau	A	2.42	M2	0.07 ± 0.06	0.13 ± 0.14	1	1	Hα	4.3	III	W	2	
	B	...	...	0.73 ± 0.11	4.27 ± 0.17	1	1	Hα	15.	II	C	2	
NTTS 155203−2338	A	[0.0]	...	0.52 ± 0.04	0.11 ± 0.06	1	1	Br γ	...	III	W	8	
	B	...	...	0.08 ± 0.09	−0.27 ± 0.05	1	1	Br γ	...	III	W	8	
WSB 18	A	2.66	M2	0.15 ± 0.24	0.86 ± 0.21	1	1	Hα	8.4	III	W	7	
	B	...	M2.5	0.49 ± 0.09	2.48 ± 0.13	1	1	Hα	140	II	C	7	
WSB 26	A	0.79	M0	0.70 ± 0.09	2.57 ± 0.14	1	1	Hα	109	II	C	7	
	B	...	M3	0.64 ± 0.08	3.77 ± 0.14	1	1	Hα	178	II	C	7	
ROX 15[d]	A	8.43	M3	0.37 ± 0.12	2.00 ± 0.10	1	1	Br γ	...	II	C	6, 8	
	B	...	M3	0.47 ± 0.08	1.75 ± 0.12	1	1	Br γ	...	II	C	6, 8	
AS 205	A	2.41	K5	0.92 ± 0.15	3.35 ± 0.18	1	1	Hα	220	II	C		
	B	...	M3	0.88 ± 0.13	3.37 ± 0.19	1	1	Hα	55	II	C		
WSB 19	A	1.68	M3	0.62 ± 0.05	4.02 ± 0.07	1	1	Hα	56	II	C	7	
	B	...	M5	0.36 ± 0.10	3.89 ± 0.12	1	1	Hα	37	II	C	7	
DoAr 24E	A	4.75	K5	0.45 ± 0.17	2.63 ± 0.18	9	1	Br γ	...	II	C	6, 8, 11	
	B	...	...	1.62 ± 0.17	5.05 ± 0.15	9	1	Br γ	...	I	C	6, 8	IRC
DoAr 26	A	1.64	M4	0.68 ± 0.26	2.41 ± 0.26	1	1	Br γ	...	II	C	6, 8	
	B	...	M6	0.10 ± 0.22	1.88 ± 0.22	1	1	Br γ	...	II	W	6, 8	Passive
WSB 28	A	3.28	M3	−0.13 ± 0.13	−0.07 ± 0.11	1	1	Br γ	...	III	W	6	
	B	...	M7	0.02 ± 0.44	2.24 ± 0.36	1	1	Br γ	...	II	W	6	Passive
S CrA	A	0.41	K3	1.40 ± 0.11	3.39 ± 0.12	1	1	Br γ	...	II	C	6	
	B	...	M0	1.33 ± 0.13	3.67 ± 0.14	1	1	Br γ	...	II	C	6	

TABLE 4—*Continued*

Object	Component	A_v[a]	Spectral Type	Dereddened $K-L$	Dereddened $K-[N]$	References[b] Mid-IR	References[b] Near-IR	Line?	EW(Hα) (Å)	T Tauri Class	T Tauri Type	References	Notes
LkCa 3	A	1.20	...	-0.02 ± 0.04	0.26 ± 0.11	1	1	...	...	III			
	B	...	...	-0.01 ± 0.05	0.07 ± 0.08	1	1	...	...	III			
HBC 411	A	6.71	...	0.65 ± 0.05	3.41 ± 0.13	1	2	...	...	II			
	B	...	...	0.45 ± 0.09	2.36 ± 0.13	1	2	...	...	II			
V853 Oph	A	0.29	...	0.56 ± 0.04	2.26 ± 0.10	1	1	...	...	II			
	B	...	...	0.46 ± 0.07	2.17 ± 0.07	1	1	...	...	II			
SR 9	A	[0.0]	...	0.62 ± 0.03	2.81 ± 0.10	1	1	Hα	10.5	II			
	B	...	...	0.36 ± 0.07	2.95 ± 0.12	1	1	Hα	13.8	II			

Note.—Table 4 is also available in machine-readable form in the electronic edition of the *Astrophysical Journal*.

[a] A_v is measured from photometry for the combined system. Values given as [0.0] indicate an assumed extinction of 0.0 mag in cases where $J-H$ and $H-K$ colors fall below the CTTS locus.

[b] If a reference is given as a fractional number, the unitary number reference corresponds to the K band and the fractional part corresponds to the L band.

[c] Hartigan & Kenyon (2003) find an EW(Hα) = 23 ± 4 Å, on the border between CTTS and WTTS. Based on this, the lack of veiling and [O I] emission, and NIR excess, they define it to be a WTTS. We use their classification here.

[d] ROX 15 flickers in accretion; Prato et al. (2003) see no Brγ in either component, whereas Greene & Meyer (1995) and Luhman & Rieke (1999) do see Brγ in the resolved system. We went with C/C because the system is seen to be accreting at least on some occasions.

References.—(1) This paper; (2) White & Ghez 2001; (3) Woitas et al. (2001); (4) Duchêne et al. 1999; (5) Hartigan & Kenyon 2003; (6) Prato et al. 2003; (7) Brandner & Zinnecker 1997; (8) L. Prato, private communication; (9) Stanke & Zinnecker 2000; (10) McCabe et al. 2003; (11) Doppmann et al. 2003.

Ghez 2001). At 18 μm we have detected two class I sources, 19 class II sources, and two class III sources. We lack the sensitivity at this wavelength to detect the majority of the WTTSs in our data set.

While the distinction between class II and class III stars remains clear in the $K-[N]$ index in Figure 1, the $K-L$ index shows some overlap. Using the Kenyon & Hartmann (1995) cutoffs, we would expect class III stars, with only photospheric emission, to have $K-L \lesssim 0.4$ and the boundary between class II and class I to be at $K-L \sim 1.5$. However, several class II objects, with clear $K-[N]$ excesses, have $K-L$ colors consistent with class III objects. One possibility is that this subset of our sample has disks with inner holes in their dust distributions.

The possibility of inner disk holes becomes even more intriguing when the accretion diagnostics are considered. Of the 58 class II stars, 52 have accretion information. While the majority of stars with IR excess (class II) are also accreting (CTTSs), we find that 11% of the observed class II stars with accretion diagnostics do not appear to be currently accreting. We define these objects to be passive disks; the star is surrounded by significant amounts of dust, most likely in the form of a disk, but material does not appear to be actively accreting onto the photosphere. These objects are highlighted in Table 4 with "Passive" in the Notes column and are discussed in more detail in Appendix D. The majority (66%) of the nonaccreting, passive disks also have $K-L$ colors that suggest the presence of an inner disk hole. A K-S test comparing the distribution of colors between the passive disks and class II CTTS sample shows that there is only a 0.9% probability (a 2.6 σ result) that they are sampling the same distribution in $K-L$. On the other hand, there is no large difference in the distributions of $K-[N]$ between class II CTTSs and the passive disks (8%, or 1.8 σ). The passive disks appear to be associated with the inner disk hole population.

There is a tendency (5/6) for the passive disks to reside in mixed systems,[10] where a WTTS is paired with a CTTS. There is also a tendency for the passive disk to be present around the secondary, the lowest mass component in the binary system. Only one passive disk is found around a primary and that is FV Tau/c A. The stellar companions to the passive disk objects appear to be normal CTTSs or WTTSs based on their $K-L$ and $K-[N]$ color indices. Because the sample of passive disks is small, neither tendency is statistically significant.

The passive disks are in binary systems that span almost the entire range of separations in the sample, from 0.″3 to 5″. The presence of a companion star in the range of binary separations probed here does not appear to affect whether a disk is passive or not. Indeed, the presence of a passive disk does not appear to be restricted to stars in binary systems. A comparison sample of known single T Tauri stars with near-infrared and mid-infrared colors available in the literature is shown in Figure 2 (see Appendix C for sample details). We now know less about the mid-infrared properties of single T Tauri stars than we do about those in multiple systems; we therefore have a limited sample size for this comparison and the majority of the single-star mid-infrared colors are based on low spatial resolution *IRAS* measurements. With these caveats in mind, we find a similar fraction of passive disk systems (1/20, or 5%) around single stars. Whatever phenomenon is responsible for the passive disks, it does not appear to be related to the presence of a wide-separation (>30 AU) stellar companion.

A closer examination of the stellar properties of the passive disk systems in our binary sample reveals that this phenomenon appears to be restricted to stars with spectral types of M2.5 and later. Dividing the class II stars into two roughly equal subsets based on whether the spectral type is earlier or later than M2.5, we find 0 out of 28 passive disks in the early spectral type set and 6 out of 22 in the late spectral type set. The distribution of spectral types for the sample of normal class II CTTS stars is compared to those of passive disks in Figure 3, which combines both the single-star sample and binary-star sample together. In this combined sample we find 0/26 passive disks for objects with spectral types earlier than M0 and 7/46 (15%) for objects with a spectral type of M0 or later. A K-S test on the two spectral type distributions shown in Figure 3 finds a 0.9% probability that these samples are drawn from the same parent distribution. Since later type stars are more chromospherically active, the Hα threshold increases with spectral type. Our correction for this employs a coarse threshold approximation for an inherently continuous distribution of upper limit chromospheric Hα equivalent widths as a function of spectral type (see § 2), raising the possibility that the nonaccretion status of these passive disks may be misclassified. We have

[10] One passive disk, WSB 28, is in a WTTS-WTTS pair.

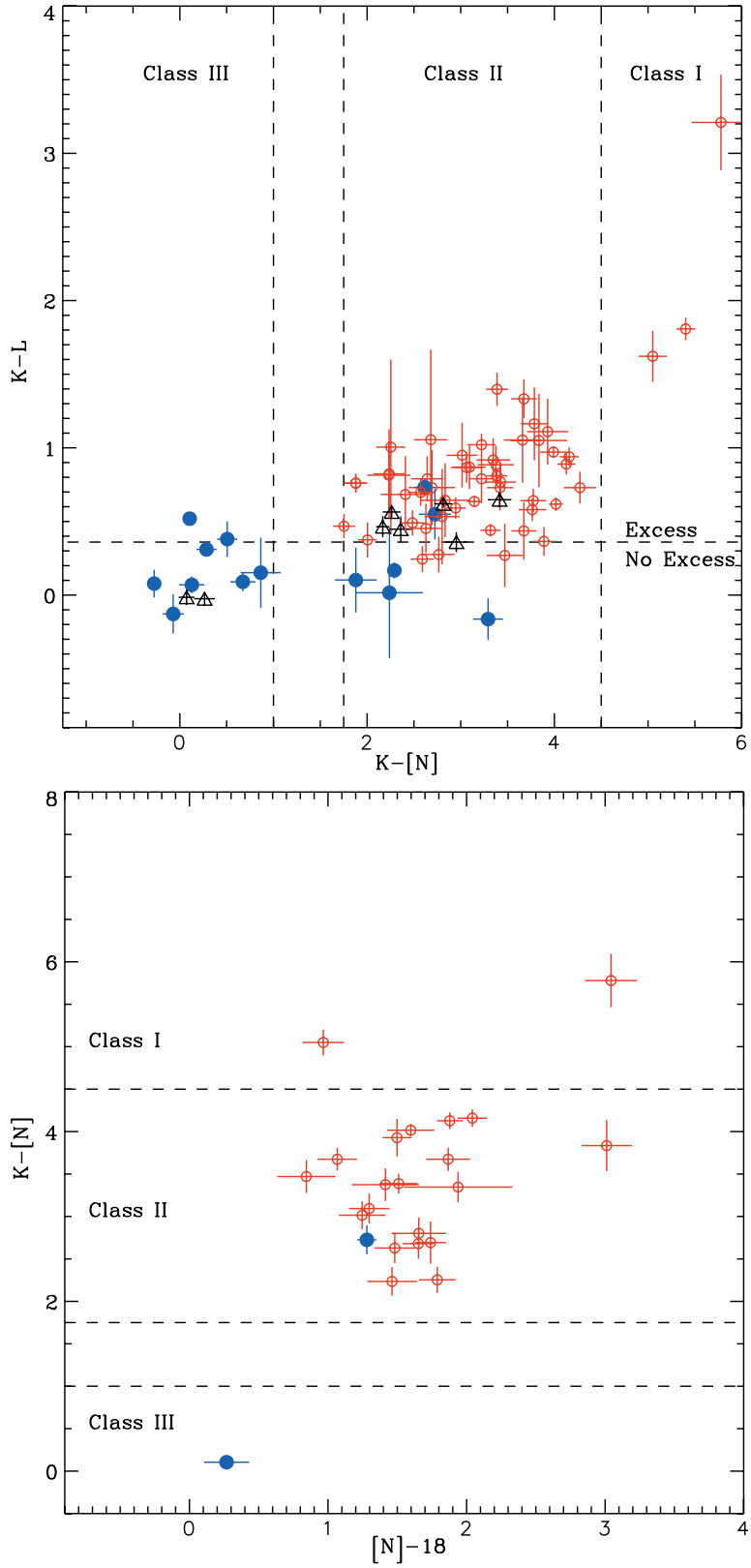

FIG. 1.—Infrared colors for our sample. *Top*: Dereddened $K - L$ vs. $K - [N]$ color plane. The symbol type represents the accretion status: actively accreting (*red open circle*), not accreting (*blue filled circle*), or accretion status unknown (*black triangle*). The $K - [N]$ color definitions for the different T Tauri classes are also shown, along with the $K - L$ color limit used to define whether the dereddened color is in excess of that expected from a photosphere. Of particular note is that 10% of the class II stars are not accreting (i.e., are passive disks) and these systems, on average, have lower $K - L$ colors than accreting class II stars. *Bottom*: Dereddened $K - [N]$ vs. $[N] - 18$ color plane, with symbol types the same as in the top panel.

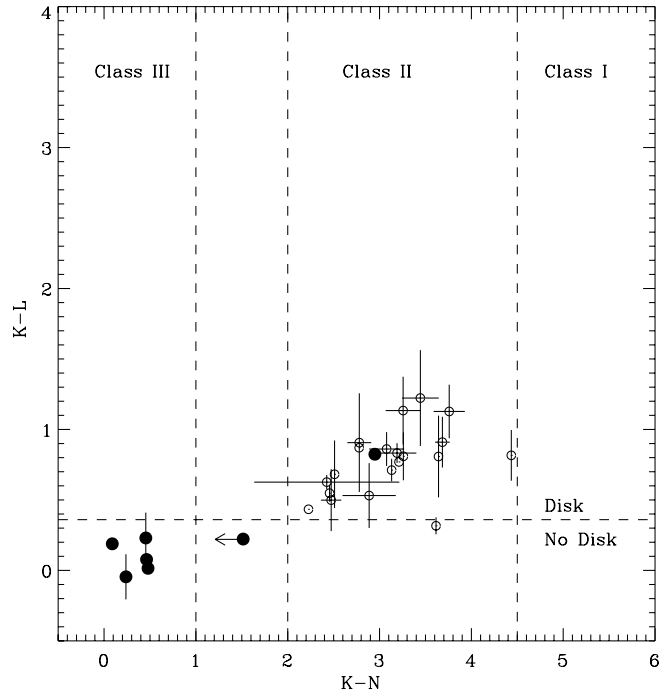

FIG. 2.—$K - L$ vs. $K - [N]$ dereddened color plane for a sample of single stars from White & Ghez (2001) and Barsony et al. (2003). Open circles represent CTTSs, whereas filled circles represent WTTSs. Of the 20 class II stars in the sample, 1 is not accreting, corresponding to a 5% detection rate of passive disks in single stars, similar to that seen in binary systems.

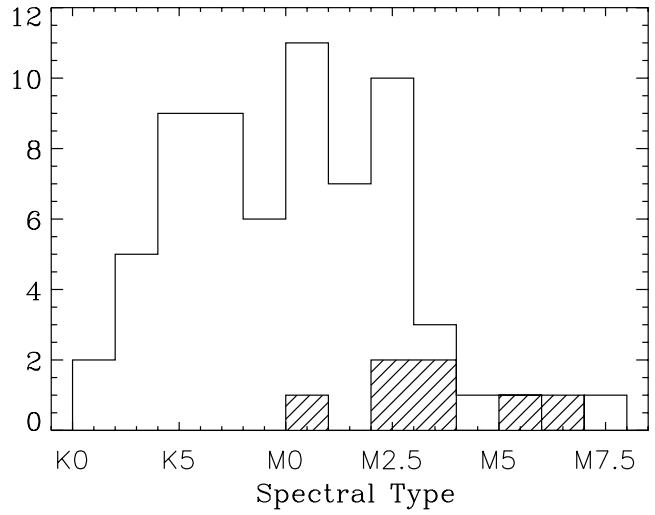

FIG. 3.—Histogram of the spectral types for all class II CTTSs in both our binary-star sample and single-star sample. For comparison, the distribution of spectral types for the passive disk stars is overplotted (*hatched region*). All passive disks are found around M-type stars, and a K-S test demonstrates that these two distributions are unlikely to have been drawn from the same parent population.

checked the passive disks that have Hα measurements to see how close to the limit the Hα level is. Although FQ Tau B is a borderline CTTS/WTTS case, LkHa 332 B, FV Tau/c A, and FX Tau B are unambiguous. These results suggest that the presence of a passive disk with an inner disk hole appears to be dependent on the spectral type, and hence mass, of the central star.

5. DISCUSSION

Approximately 10% of all class II T Tauri stars, with significant evidence for a circumstellar disk at 10 μm, do not appear to be currently accreting. Previous work has shown that the accretion flow in T Tauri stars is quite variable (e.g., Smith et al. 1999; Alencar et al. 2001; Alencar & Batalha 2002; Littlefair et al. 2004), suggesting that a misidentification of WTTS/CTTS status can occasionally occur. If what we are observing is entirely the result of a stochastic accretion process, then the sample of observed passive disk stars suggests that, on average, class II stars spend approximately 10% of their CTTS lifetime in a nonaccreting state. As we point out in Appendix D, a couple of the candidate passive disk objects may in fact be undergoing stochastic accretion. However, a variable accretion flow cannot account for the observed link between a nonaccreting disk and the presence of an inner disk hole or the observed spectral type/mass dependence. In the following subsections we explore two mechanisms that can reproduce the observed inner disk hole in the passive disk systems: (1) the presence of a nearby, as yet unresolved companion (either stellar or substellar/planetary in mass; § 5.1), or (2) disk evolution (§ 5.2).

5.1. *Evidence for Unresolved Companions?*

In principle, the presence of a nearby companion could reproduce the observed inner disk hole and, potentially, the lack of significant accretion through star-disk or planet-disk interactions. Such companions could not have been imaged around the passive disk systems in our sample as they would have been too close to resolve, and radial velocity monitoring of these objects has, to the best of our knowledge, not been done. In systems with a stellar companion (with mass ratios $\lesssim$10), resonances between the orbit of the star (with semimajor axis a) and that of the dust in the disk will dynamically clear out material up to $2a$–$3a$, depending on the eccentricity of the orbit (Artymowicz & Lubow 1994). For planetary mass companions it is generally assumed that the disk clearing occurs essentially at the apoastron of the planet's orbit (e.g., Quillen et al. 2004). Because the near-infrared and mid-infrared excesses arise from the inner few AU of the disk, only systems with companions at separations on order of 1 AU could lead to the absence of such excesses. Consistent with these predictions, observed spectroscopic binaries with separations less than $\sim$0.3 AU do not show the characteristics of the passive disk systems; they have $K - L$ excesses and accretion can still occur across the disk gap (e.g., DQ Tau, Mathieu et al. 1997; AK Sco, Alencar et al. 2003; NTTS 162814−2427, Jensen & Mathieu 1997), whereas there are two systems with either known or putative companions at separations on the order of a few AU that would be classified by us as passive disks: HD 98800 B (K5 combined spectral type), which has a *known* stellar companion at an apoapstron distance of 1.6 AU (e.g., Koerner et al. 2000; Prato et al. 2001), and CoKu Tau 4 (an M1.5 star), whose spectral energy distribution has been modeled assuming an *undetected* companion with $M > 0.1 M_{\rm J}$ at 10 AU (Quillen et al. 2004; D'Alessio et al. 2005). Thus, companions with separations on order of 1 AU are capable of mimicking the color and accretion properties of the passive disk systems.

While a stellar or substellar companion a few AU from the star could be responsible for the observed lack of accretion and presence of an inner disk hole, companions are unlikely to be the explanation for all the observed passive disks. The period distribution for stellar companions to M-type dwarfs (for separations $\lesssim$10 AU) is very similar to that around G- and K-type dwarfs, with approximately 10% of the stars having a companion in the 0.3–3 AU separation range (Duquennoy & Mayor 1991; Marchal et al. 2003). If all the passive disks were caused by a stellar companion in this separation range, we would be equally likely to find passive disks around K-type stars as M-type stars in our sample, which is

not the case. The observed mass dependence also suggests that *sub*stellar or planetary companions are not the probable cause. As Butler et al. (2004) show, planets with separations $\lesssim$1 AU are $\sim$5 times less likely to occur around M-type stars than around G- or K-type stars. Therefore, the fact that all the passive disks occur solely around M-type T Tauri stars makes the presence of a companion, either stellar or substellar, an unlikely explanation for the group as a whole.

5.2. *Evidence for "Inside-Out" Disk Evolution*

The transition from the class II to the class III stage has been the focus of a number of recent theoretical investigations. Different physical processes that could be responsible for disk evolution will produce different signatures in the color plane as a function of time. There are three classes of models that we investigate here. The first is the homologous disk evolution of Wood et al. (2002), in which the disk structure remains constant and the only property that evolves is the disk mass. The second is the magnetospheric disk accretion models, which investigate the viscous evolution of disks in the presence of magnetospheric interactions between a disk and a star (e.g., Kenyon et al. 1996; Armitage et al. 1999). Finally, there are models in which the disk evolution is driven by the competing effects of the ionizing flux from the central star, which creates a disk wind, and the viscosity (Hollenbach et al. 1994; Clarke et al. 2001). In this section we use the observed properties of the passive disk systems to constrain which model (and associated physical processes) is most likely responsible for disk evolution. The observed passive disk properties we use are (1) the evidence for an inner disk hole, as determined through photospheric $K - L$ colors and optically thick, disklike $K - N$ colors; (2) the fact that these systems only occur around M-type stars; and (3) the observed fraction of such systems: 10% of the entire class II sample (including both singles and binaries), or, more accurately, 0% for K-type class II stars and 15% for M-type class II stars.

Wood et al. (2002) model the near- and mid-infrared colors of a typical T Tauri disk under the assumption that the disk evolves through a reduction in the disk mass while maintaining a constant disk structure. They find that the observed spread of $K - L$ and $K - N$ colors can, in general, be reproduced by disks of different masses observed at varying disk inclinations. However, Wood et al. (2002) point out that the constant disk structure in this model assumes that disks with inner holes will not develop as the disks evolve. With $\sim$10% of our class II stars showing evidence for an inner disk hole, we can reject this model.

Models that investigate the viscous evolution of magnetospheric T Tauri disks (e.g., Kenyon et al. 1996; Armitage et al. 1999) find that disks evolve in an inside-out manner. The radius of the inner edge of a magnetically truncated disk is determined by the balance between the magnetic torques and viscous torques in the disk. As the system ages and the mass accretion rate drops, the radius at which this balance occurs increases; hence, an inner disk hole forms and evolves with the mass accretion rate and magnetic field strength. The disks are predicted to evolve in the $K - L$ versus $K - N$ color plane through a phase with photospheric $K - L$ and disklike $K - N$ colors, suggesting that the passive disk systems could represent a population that is in the process of dispersing their inner disk material. Hartmann (1998) shows that the size of the inner disk hole is dependent on a number of parameters (such as stellar radius, accretion rate, and magnetic field strength), most of which are themselves dependent on the stellar mass. Because of the complexity in the interplay between the parameters, the exact dependence remains unknown, however, and so the presence of a spectral type dependence in the observations, while not inconsistent with this model, cannot currently constrain it. The model does fail, however, to accurately predict the observed fraction of such systems in the sample as a whole. In this model, disk evolution is driven by the decline in accretion rate over time and occurs on the viscous timescale of the entire disk (which scales with the outer radius of the disk and viscosity parameter as $R_{\rm outer}^2/\nu$). Calculations of the observed disk colors as a function of time predict that roughly 50% of all class II stars should be detected with photospheric $K - L$ colors and $K - N > 2$, a factor of 5 too large compared to our observations.

Clarke et al. (2001) investigate disk evolution with the inclusion of disk photoevaporation. An ionizing flux from the central star creates a disk wind that is launched beyond some critical radius, $R_g = GM_*/c_s^2$. As the mass accretion rate declines with time, there comes a point when the mass loss in the disk wind at R_g exceeds the mass accretion into the disk region inside that radius. The lack of replenishment in the inner disk region causes it to evolve on its own short viscous timescale, producing a rapid removal of material (Clarke et al. 2001; Armitage et al. 2003). This provides the potential for a rapid transition in disk evolution, with the inner disk region clearing out on a timescale on the order of 10^5 yr for a 1 $M_\odot$ T Tauri star. The removal of material at radii smaller than R_g after the mass accretion rate has declined yields photospheric colors at wavelengths shorter than some critical value and optically thick colors at longer wavelengths, with the critical wavelength depending only on the size of the inner disk hole. In Clarke et al. (2001) the photoionizing photons from the central star were assumed to have a constant flux over time. They state that the source of ionizing photons cannot be predominantly powered by the accretion flow because as the accretion rate drops over time, this process will essentially become ineffective. Indeed, Matsuyama et al. (2003) show that if the source of ionizing flux is from the accretion shock, with the flux declining over time, a disk gap around R_g forms but the inner disk does not clear out any faster than the outer disk. More recently, Alexander et al. (2004a, 2004b, 2005) have explored alternative, constant sources of ultraviolet (UV) photons and have concluded that chromospheric far-UV photons in T Tauri stars potentially can provide a high enough flux, causing the inner disk to rapidly clear once the accretion rate drops. Within this scenario, our sample of passive disks can be interpreted as objects that have already undergone inner disk clearing. The observed fraction of passive disks around M-type stars (15%) suggests that this phase of disk evolution, with a cleared inner disk region, lasts for several times 10^5 yr. This model also predicts a strong dependence on the mass of the central star as the disk radius at which a disk wind can be launched scales linearly with the stellar mass. The Clarke et al. (2001) model predicts that while a 1.5 $M_\odot$ star will have an inner disk hole out to 10 AU, a 0.25 $M_\odot$ star will have an inner disk hole that extends out to only 1–2 AU. Consequently, the reason we detect passive disks solely around M-type stars is purely a selection effect: because our survey covers only the 2–10 μm region, we can only detect disk holes up to $\sim$3 AU in size. We would detect a 1.5 $M_\odot$ star with a larger disk hole as a class III, diskless object. In this framework, we therefore predict that *Spitzer* observations across the 3–160 μm region will identify a number of systems with 5–15 AU inner disk holes around G and K T Tauri stars, and that the size of the inner hole will scale linearly with the stellar mass. Furthermore, a direct consequence of the linear relation between stellar mass and inner hole size is that the timescale required for the inner disk region to clear is also dependent on the stellar mass. This is because the inner disk clears on its own viscous timescale, which scales as R_g^2/ν. We therefore predict a higher likelihood of detecting objects in the process of clearing

their inner disk around higher mass T Tauri stars, a prediction that can be tested with *Spitzer*.

To summarize, the homologous disk evolution of Wood et al. (2002) can be discounted by the detection of the passive disk systems with inner disk holes, and models of magnetospheric disk evolution that evolve on a purely viscous timescale cannot recreate the small fraction of observed passive disks. However, models that incorporate the effects of both viscous evolution and disk photoevaporation can recreate all the observed properties of these systems.

While the disk photoevaporation evolution models seem to be successful at describing the evolution of the inner edge of the disk, the evolution of disk material farther out is still not well understood. Beyond the disk wind launch radius, disk material remains and continues evolving on a viscous timescale (Clarke et al. 2001). In star-forming regions where external photoionization does not cause the disk to evolve in an outside-in manner, the models predict a remaining outer disk annulus of gas and dust. However, millimeter surveys of T Tauri stars find that only $\sim$10% of all WTTSs have associated millimeter continuum emission (e.g., Duvert et al. 2000; Osterloh & Beckwith 1995). The disk evolution timescale therefore does not seem to have a strong radial function. Recent work by Takeuchi et al. (2005) suggests that the solution may be the differential radial motion of dust grains and gas particles in circumstellar disks; for T Tauri disks with 1 mm grain sizes, the dust particles should migrate inward on a timescale an order of magnitude faster than the gas; by the time the disk has started the inside-out evolution process, the outer disk is already depleted of dust grains, leaving a gas-rich disk behind. It is clear that investigating the outer disk structure of candidate passive disks, in both dust and gas emission, will help explore this idea further. Our 18 μm data do not have the sensitivity to investigate this question; of the four candidate passive disks observed at 18 μm in our sample, only one system was wide enough and bright enough to provide resolved photometry for each component. For FX Tau B, the passive dust disk does seem to extend out to farther radii. Future deep mid-infrared images of these systems will be able to pinpoint the radial distribution of small dust grains.

6. SUMMARY

Mid-infrared and near-infrared observations of a sample of 65 binary systems are presented, increasing the number of T Tauri binary systems with resolved 10 μm data by a factor of 5. We have discovered a sample of class II stars, with clear evidence for optically thick disk emission in the mid-infrared, that do not appear to be currently accreting. The majority of these passive disks have an inner disk hole, determined through the lack of near-infrared excess, and all of them occur only around the lowest mass stars (M type) in our sample. These observations are consistent with models that include inside-out disk evolution. In particular, the observed frequency and spectral type/mass dependence of the passive disk systems, in the 2–10 μm region covered in this survey, are supportive of models that include a photoevaporative disk wind caused by an ionizing flux from the central star. A strong prediction of the photoevaporation models is that there should be a sample of systems with larger inner disk holes (5–10 AU) around higher mass stars, with the size of the disk hole scaling with stellar mass. Such systems would not be detectable in the 2–10 μm study presented here; a multiwavelength mid-infrared study of T Tauri stars, which will be available through *Spitzer*, will be able to determine whether photoevaporative disk wind models can adequately describe T Tauri disk evolution over a range of stellar masses.

A portion of this research was done while the author held a National Research Council Research Associateship Award at the Jet Propulsion Laboratory. We are grateful to Cathie Clarke for helpful comments, to Robert Piña for his assistance with OSCIR observations, and to the referee for a careful reading of this work. Some of the data presented herein were obtained at the W. M. Keck Observatory, which is operated as a scientific partnership among the California Institute of Technology, the University of California, and the National Aeronautics and Space Administration. The Observatory was made possible by the generous financial support of the W. M. Keck Foundation. Support for this work was provided by the NASA Astrobiology Institute and the Packard Foundation. This publication makes use of data products from the Two Micron All Sky Survey, which is a joint project of the University of Massachusetts and the Infrared Processing and Analysis Center/California Institute of Technology, funded by the National Aeronautics and Space Administration and the National Science Foundation. The authors also wish to recognize and acknowledge the significant cultural role that the summit of Mauna Kea has always had within the indigenous Hawaiian community. We are fortunate to have the opportunity to conduct observations from this mountain.

APPENDIX A

LINE-OF-SIGHT EXTINCTION

Typically, the line-of-sight extinction to a star is estimated by measuring the excess color of the star, in comparison to that expected from the photosphere, in bandpasses that are dominated by photospheric emission rather than disk emission. Such a method is not open to us; we lack spectral types for each individual star in approximately 40% of the binary systems in our sample. Furthermore, a number of these systems have not been resolved at optical (R or I band) wavelengths where the photosphere dominates the flux density. Instead, a secondary method of determining extinction was applied. Meyer et al. (1997), using the sample of T Tauri stars from Strom et al. (1989), found that the CTTSs, dereddened using A_v determined from the $R - I_c$ excesses, defined a narrow locus in the $(J - H)_{\rm CIT}$ versus $(H - K)_{\rm CIT}$ color-color plane. We therefore compared the near-infrared colors of the observed binary systems with the CTTS locus defined by Meyer et al. (1997) in order to estimate the line-of-sight extinction.

Using the 2MASS database, J, H, and K photometry was obtained for stars in the sample. For most stars, the 2MASS data do not resolve the binary components and therefore provide composite fluxes only. The magnitudes obtained from 2MASS were converted into CIT magnitudes using the filter transformations from Carpenter (2001). Using the equation in § 3.1 of Prato et al. (2003), which relates the visual extinction with the distance between the CTTS locus and the stellar position in the $(J - H)_{\rm CIT}$ versus $(H - K)_{\rm CIT}$ color-color diagram, the visual extinction, A_v, was calculated for each binary system in our sample. The A_v values calculated using this method are given in Table 4. A few stars did not have 2MASS photometry and some (18% of sample) had initial positions that were below the CTTS locus, possibly the result of scattering from circumstellar material or photometric variability. As the A_v values cannot be determined in this case, we

TABLE 5
Flux Densities of Calibrators

Name	OSCIR (Jy)		LWS (Jy)		
	N	IHW18	8.8 μm	12.5 μm	SiC
Primary Calibrators					
α Lyr	33.99	11.96	49.26	24.96	28.24
ρ Boo	20.81	7.52	28.23	15.72	17.8
γ Aql	66.11	24.29	89.2	50.47	56.78
α Boo	619.12	219.21	877.25	457.78	520.11
α Ari	68.8	24.93	95.37	51.72	58.52
β Peg	323.50	122.23	439.96	246.84	278.75
10 And	5.07	1.87	6.73	3.91	4.42
HD 27482	5.95	2.33	7.86	4.78	5.25
HD 1240	8.35	3.08	11.08	6.44	7.27
Secondary Calibrators					
α CrB	4.24 $\pm$ 0.25	1.35 $\pm$ 0.01	6.36 $\pm$ 0.6	3.3 $\pm$ 0.2	...
α CMi	69.73 $\pm$ 5.38	23.1 $\pm$ 0.6	...	...	53.88 $\pm$ 0.58
α Sco	[2269]	[815.75]	...	...	...
δ Sco	6.09 $\pm$ 0.9	2.89 $\pm$ 0.3	...	...	...
μ UMa	[96.46]	[34.02]	...	...	...
SAO 90816	11.03 $\pm$ 0.9	3.56 $\pm$ 0.1	...	...	...

have arbitrarily set them to have $A_v = 0.0$. The observed mid-infrared and near-infrared colors are dereddened using the Rieke & Lebofsky (1985) extinction coefficients for the K-, L-, and [N]-band fluxes and using the 18 μm extinction coefficient from Allen's Astrophysical Quantities.

APPENDIX B

ABSOLUTE PHOTOMETRIC CALIBRATION

During each night's observations, a number of photometric standards were observed. While these standards have known flux densities for a number of mid-infrared filters, this project has used a large number of both broadband and narrowband filters that differ slightly from those in the literature. We have therefore recalibrated the standards in each of the filters used. The standards can be split into two groups: "primary" standards that have absolutely calibrated photometry and a template stellar spectra, available through the Cohen-Walker radiometric network (Cohen et al. 1992, 1995, 1999), and "secondary" standards that have their absolute calibration estimated through relative photometry with any primary calibrators observed on the same night.

Absolute calibration of the primary standards was done by taking the published, absolutely calibrated, stellar templates and integrating the stellar spectra (F_λ) through the filter bandpass (B_λ), the instrument detector QE (DQE), and the atmospheric transmission ($T_{\rm atmos}$):

$$F_{\rm filter} = \int \frac{F_\lambda T_{\rm atmos}({\rm DQE}) B_\lambda}{T_{\rm atmos}({\rm DQE}) B_\lambda}\, d\lambda.$$

DQE and filter transmission curves for the LWS and OSCIR instruments were provided by R. Campbell and S. Fisher, respectively. The model atmosphere used is the ATRANS atmospheric transmission model by Lord (1992) and includes 1 mm of precipitable water. These models are available on the Gemini Web site.[11] Models with precipitable water varying from 1 to 5 mm were tested. For all bandpasses used in this study, changing the atmospheric water content changed the total weighted flux by less than 1%, well below the observational uncertainties of the data. The resulting flux densities for these primary photometric calibrators, in janskys, are reported in Table 5 for each filter used. Using the subset of the observed standards that also have fluxes estimated by the OSCIR team to compare the measured zero points, we find that the flux densities are consistent to within $\sim$6% and $<$1% for the N-band filter and IHW18 filter, respectively.

The secondary standards are calibrated through relative photometry to primary standards that are observed on the same night, under photometric conditions. The observed flux ratios are converted into fluxes using the primary standard fluxes. The average and standard deviation of the measured fluxes for the secondary standards are also provided in Table 5. For those standards observed only during nonphotometric nights we have adopted the OSCIR team's photometry, if available. These are indicated by fluxes placed inside square brackets.

[11] See http://www.gemini.edu/sciops/ObsProcess/obsConstraints/ocTransSpectra.html.

TABLE 6
SINGLE STARS

Star	Spectral Type	A_v	Observed[a]			EW(Hα) (Å)	EW(Hα) References	Multiplicity References	T Tauri		Observation Method	Notes
			$K-L$	$K-[N]$	References				Class	Type		
GM Aur.....	K3	0.25	0.33 ± 0.06	3.63	1	96	5	10	II	C	Speckle	
CW Tau.....	K3	1.22	1.20 ± 0.24	3.33 ± 0.19	1	135	5	9, 10	II	C	Speckle	
DS Tau	K5	0.00	0.71 ± 0.08	3.13	1	59	5	10	II	C	Speckle	
LkCa 15	K5	0.41	0.57 ± 0.06	2.48	1	13	5	10	II	C	Speckle	
BP Tau	K7	0.72	0.57 ± 0.23	2.93 ± 0.29	1	40	6	9	II	C	Speckle	
GK Tau	K7	0.32	0.85 ± 0.07	3.21 ± 0.21	1	22	7	9	II	C	Speckle	
AA Tau.....	K7	0.72	0.90 ± 0.12	3.12 ± 0.19	1	37	5	10	II	C	Speckle	
DL Tau	K7	0.00	1.21 ± 0.34	3.43 ± 0.20	1	105	5	10	II	C	Speckle	
GI Tau.....	K7	0.93	0.96 ± 0.18	3.74 ± 0.08	1	20	7	9, 10	II	C	Speckle	
CI Tau	K7	1.68	0.90 ± 0.17	3.36	1	102	5	9, 10	II	C	Speckle	
DN Tau	M0	0.95	0.55 ± 0.22	2.53 ± 0.11	1	12	5	10	II	C	Speckle	
IP Tau.....	M0	0.37	0.89	2.80	1	11	5	10	II	C	Speckle	
DO Tau	M0	1.52	1.21 ± 0.19	3.85 ± 0.17	1	100	5	9, 10	II	C	Speckle	
DP Tau	M0.5	2.63	0.95 ± 0.29	3.80	1	85	5	10	II	C	Speckle	
DE Tau.....	M1	1.18	0.97 ± 0.35	2.85 ± 0.13	1	54	6	9	II	C	Speckle	
DM Tau.....	M1	0.25	0.83 ± 0.18	4.45	1	139	5	10	II	C	Speckle	
FM Tau	M1	0.33	0.70 ± 0.24	2.53	1	62	7	10	II	C	Speckle	
DH Tau	M2	0.25	0.64 ± 0.05	2.44 ± 0.79	1	72	7	9	II	C	Speckle	
V827 Tau	K7	0.00	0.10 ± 0.18	0.31	1	1.8	5	10	III	W	Speckle	
LkCa 4	K7	1.03	0.18	0.08	1	5	6	10	III	W	Speckle	
HBC 374.....	K7	2.45	0.01 ± 0.16	0.30	1	3	6	9, 10	III	W	Speckle	
V819 Tau	K7	2.52	0.21	0.61	1	1.7	6	9, 10	III	W	Speckle	
IQ Tau.....	M0.5	1.02	0.96	3.1	1	8	5	9, 10	II	W	Speckle	Passive
LkCa 1	M4	1.30	0.07	0.54	1	4	5	10	III	W	Speckle	
SR 4	K5	1.25	0.84	3.29	2, 3	84	5	9, 11	II	C	Speckle/lunar	
ROX 7.....	K7	6.23	0.29	<1.59	3	1.5	8	12	...	W	Speckle	
ROX 44.....	K3	0.90	0.77	2.6	4	54	5	11, 13	II	C	Speckle/lunar	

[a] Uncertainties in the observed colors are given when available in the literature.

REFERENCES.—(1) Kenyon & Hartmann 1995; (2) Myers et al. 1987; (3) Wilking et al. 1989; (4) Rydgren et al. 1976; (5) Herbig & Bell 1988; (6) Strom & Strom 1994; (7) Hartigan et al. 1994; (8) Bouvier & Appenzeller 1992; (9) Ghez et al. 1993; (10) Leinert et al. 1993; (11) Simon et al. 1995; (12) Ageorges et al. 1997; (13) Barsony et al. 2003.

Throughout this paper we assume that α Lyr has 0.00 mag in each bandpass used. While Vega does have a circumstellar shell, the excess emission from this dust does not occur at wavelengths shorter than 20 μm (e.g., Cox 2000).

APPENDIX C

KNOWN SINGLE T TAURI STARS

A comparison sample of T Tauri stars that have been determined to be single has been compiled from Table 7 from White & Ghez (2001) for Taurus sources and from Barsony et al. (2003) for Ophiuchus sources. We only include sources that have their single status determined using high-resolution observations, including speckle interferometry (Leinert et al. 1993; Ghez et al. 1993; Ageorges et al. 1997; Barsony et al. 2003) and lunar occultation and imaging (Simon et al. 1995). A literature search on these known single stars was made in order to obtain *K*-, *L*-, and *N*-band information, as well as accretion information from either Hα or Brγ line emission. The total sample is comprised of 27 objects that have near- and mid-infrared disk color indices, an Hα measurement of accretion, and an estimate of the visual extinction from 2MASS photometry. These are listed in Table 6, along with the spectral type, estimated visual extinction (see Appendix A for method), observed colors, and equivalent width of Hα line emission for the star. The reference source for multiplicity is given in the ninth column, and the observational method used is listed in the twelfth column.

APPENDIX D

THE PASSIVE DISK CANDIDATES

In this appendix we provide a summary of each passive disk candidate presented in this work, identified through the observed combination of a class II–like $K-[N]$ excess and lack of accretion. As pointed out in § 5, our analysis rests on the statistical nature of this subset as a whole; however, for any one of these objects the observed properties may be caused by one of the other possibilities we have raised (i.e., varying accretion flow, the presence of a nearby companion).

WSB 28.—This 5″ binary system in Ophiuchus is one of the smallest mass ratio systems ($q \sim 0.1$, according to the tracks of Baraffe et al. 1998, 2003) in our sample. It is also the only nonmixed binary system that contains a passive disk; both components are WTTSs as indicated by a lack of Brγ emission (Prato et al. 2003). No Hα equivalent widths have been measured for either individual component.

Wilking et al. (1987) do, however, list the primary as having a weak Hα measurement. *K*-band photometry of the primary has been obtained on three separate occasions, including this work; the object appears to be photometrically stable ($\sigma_K = 0.03$ mag; standard deviation from 2MASS; Prato et al. 2003 and this work). Along with Prato et al. (2003), we have obtained *K*-band photometry on the secondary; this component also appears stable within the observational uncertainties. There are a number of line-of-sight extinction measurements, obtained using different methods; the CTTS locus method applied here finds an A_v of 3.3 mag for the system as a whole, similar to that found by Bontemps et al. (2001; $A_v = 4.3$ mag). Both combined measurements are intermediate in value between the A_v determined for each individual component, measured by spectral fitting, which finds an A_v of 5.1 $\pm$ 0.6 and 2.5 $\pm$ 1 mag for the primary and secondary, respectively (Prato et al. 2003). Dereddening the observed colors with any of the above A_v measurements does not change the classifications for each object; the primary continues to have no excess in either $K - L$ or $K - [N]$, whereas the secondary, while lacking a $K - L$ excess, shows $K - [N] > 2$, indicating that this object may have an inner disk hole. While the observational uncertainties on the color of the secondary are fairly large, it would take a 3.4 σ change for the object to fall in the class III region and cease to be regarded as a passive disk.

DoAr 26.—This M4/M6 2.″2 binary system is a mixed pair: the primary is a CTTS [EW(Brγ) = 2.2 Å] and the secondary a WTTS (nondetection of Brγ; Prato et al. 2003). No Hα measurements that resolve both components are available; the Wilking et al. (1987) Hα survey qualitatively measures an Hα level of 2 (on a scale of "weak" to "5") for the combined binary system. A comparison of all resolved ground-based near-infrared photometry on this binary system finds that the *K*-band flux of both components is stable, with an rms of 0.1 mag for each component (Koresko 2002; Prato et al. 2003; this work). Resolved *L*-band magnitudes of this system are provided only by Koresko (2002) and this work. Koresko (2002) finds $K - L = 0.7 \pm 0.3$ for the secondary, which differs by 2 σ from the value we find and is associated with much larger observational uncertainties. Additional, near-simultaneous, *K*- and *L*-band measurements are desirable to explore how variable this system is. The A_v toward the system as a whole, measured using the CTTS locus method, is 1.64 mag, intermediate between the values measured from spectral fits for the primary and secondary ($A_v = 3.3 \pm 1.2$ and 1 ± 0.9 mag, respectively; Prato et al. 2003). The dereddened $K - [N]$ colors of this CTTS-WTTS system are class II–like for both objects; the class II classification does not change no matter which A_v measurement listed above is used. The dereddened $K - L$ colors clearly indicate an excess for the primary and none for the secondary. While the primary is clearly a class II CTTS object, the secondary shows evidence for an inner disk hole and a lack of accretion.

FQ Tau.—This system appears to be highly variable. Hartigan & Kenyon (2003) find that it is an M3/M3.5 0.″73 binary, with both components showing Hα in emission, with an equivalent width of 110 $\pm$ 5 and 23 $\pm$ 4 Å for the primary and secondary, respectively. On the basis of Hα alone, the secondary would be classified as a borderline CTTS/WTTS. Hartigan & Kenyon (2003), however, also use the lack of [O I] line emission and veiling in the secondary to classify FQ Tau B as a WTTS, which is the designation we use here. Photometrically, this system varies considerably, with the brightest component at both *K* and *L* band inverting between the results presented in White & Ghez (2001) and those in Table 3. During 1997, White & Ghez (2001) found the southwestern component to be the brightest at 2.2 μm, with observed (and not dereddened) near-infrared colors of $K - L = 0.43 \pm 0.11$ and 0.37 ± 0.11 mag for the primary and secondary, respectively. In comparison, during 2001, we found the northeastern component to be brighter by $\sim$0.3 mag in the *K* band, with observed (not dereddened) near-infrared colors of $K - L = 0.61 \pm 0.07$ and 0.75 ± 0.06 mag for the primary and secondary, respectively. The A_v measurement using the CTTS locus ($A_v = 0.35$ mag) is smaller than those measured from a fit to the optical spectra ($A_v = 1.95$ and 1.8 mag for the primary and secondary, respectively; Hartigan & Kenyon 2003). The dereddened $K - [N]$ colors are class II for both components, as are the $K - L$ colors; no evidence for an inner disk hole is found using our more recent *K*- and *L*-band photometry. Dereddening with either set of A_v measurements does not change the classification for either component. We consider this object to be a borderline candidate passive disk and recommend follow-up observations.

FX Tau.—Duchêne et al. (1999) resolved the individual components in this 0.″85 binary system spectroscopically, finding spectral types of M1 and M4 for the primary and secondary, respectively, with an uncertainty of two subclasses for each designation. They found an Hα equivalent width of 13 and 1 Å for the primary and secondary, respectively, indicating that this is a mixed CTTS-WTTS binary system. The resolved Hα measurements are consistent with previous Hα measurements on the combined binary system (14.5 Å; Kenyon et al. 1998); Paβ and Brγ are also seen in emission (Muzerolle et al. 1998; Folha & Emerson 2001). The resolved *K*-band photometry used is from White & Ghez (2001), which provides an average of all resolved magnitudes available in the literature. As such, the observed $K - L$ color given in Table 3 was not derived from simultaneous measurements. Our observed *L*-band magnitudes, 7.6 ± 0.05 and 8.65 ± 0.06 mag for primary and secondary, respectively, agree well with the White & Ghez (2001) measurements (7.49 ± 0.1 and 8.67 ± 0.1 mag, respectively). The line-of-sight extinction, measured using the CTTS locus method, has an A_v of 2.24 mag, similar to the value ($A_v = 1.08$ mag) measured from the optical colors given in Kenyon & Hartmann (1995). The dereddened $K - L$ and $K - [N]$ colors in Table 4 are clearly class II colors, suggesting that this object may be in fact undergoing variable accretion as discussed in § 5.

LkHa 332.—The 0.″34 binary system was spectroscopically resolved by Hartigan & Kenyon (2003) into a K7/M2.5 pair, with Hα equivalent widths of 10.9 ± 0.6 and 6.2 ± 0.6 Å, respectively, making it a CTTS-WTTS mixed pair, although the CTTS classification for the primary is borderline. This object appears to undergo significant variation in Hα emission; previous narrowband Hα WFPC2 observations found equivalent widths of 45 and 17 Å for the primary and secondary, respectively, which, again, would classify it as a CTTS-WTTS pair (White & Ghez 2001). However, classification of this object in the literature is inconsistent. Both Hartigan & Kenyon (2003) and White & Ghez (2001) classify this binary system as a CTTS-CTTS. According to Tables 3 and 4 in Hartigan & Kenyon (2003), veiling is not present at a >2 σ level in either component (note that this is contrary to their Table 7, which states that it is present for the secondary component; we assume that this is a typo). The only emission-line evidence for active accretion in the secondary is the presence of the [O I] λ6300 line, which is strangely absent in the CTTS primary. Further spectroscopic follow-up on this close binary system is needed. Using the Hα measurements, we refer to this as a CTTS-WTTS system. For calculating the near-infrared color, we have combined the 1997 *K*-band measurement of this object from Woitas et al. (2001) with the *L*-band average measurement provided by White & Ghez (2001); we do this rather than use an average *K*-band measurement to minimize any photometric variability. This provides an observed $K - L$ color of 1.06 ± 0.1 and 0.03 ± 0.14 mag for the primary and secondary, respectively. The average observed $K - L$ colors from Woitas et al. (2001) for these objects (0.97 ± 0.11 and 0.32 ± 0.31 mag, respectively) show that

photometric variability is likely present; near-simultaneous K- and L-band photometry on this system would clearly be useful. The line-of-sight extinction estimated through the CTTS locus method is $A_v = 3.58$ mag, which is approximately 1 mag larger than the A_v found through a fit to the spectroscopic data by Hartigan & Kenyon ($A_v = 2.8$ and 2.3 mag for the primary and secondary, respectively). The dereddened colors find clear $K - [N]$ excesses in both components, independent of the A_v measurement used. The $K - L$ color of the secondary, however, shows evidence for an inner disk hole, although the lack of simultaneous measurements places some uncertainty on this.

FV Tau/c.—A 0.″67 binary system, FV Tau/c has been spectroscopically resolved into an M2.5/M3.5 pair by Hartigan & Kenyon (2003). The system appears to be a mixed WTTS–class I pair, which is quite unusual, with the WTTS designation for the primary coming from Hα equivalent width measurements and the lack of veiling and [O I] emission (White & Ghez 2001; Hartigan & Kenyon 2003). The secondary has very large and variable Hα equivalent widths (White & Ghez 2001; Hartigan & Kenyon 2003), and White & Ghez (2001) classify it as a high-accretion star. We combine the 1995 K-band measurement from Woitas et al. (2001) with the average L-band photometry from White & Ghez (2001) in order to minimize the uncertainty from photometric variability; these colors do not represent near-simultaneous measurements. The A_v estimated from the CTTS locus method is 5.23 mag, a value in between the measured A_v from a fit to the optical spectra by Hartigan & Kenyon (2003), who find $A_v = 3.25$ and 7 mag for the primary and secondary, respectively. The dereddened $K - [N]$ colors are class II and class I for the primary and secondary, respectively, independent of the A_v measurement used, whereas the $K - L$ colors of the primary are below the $K - L$ photospheric cutoff used, suggesting the presence of an inner disk hole.

REFERENCES

Ageorges, N., Eckart, A., Monin, J.-L., & Ménard, F. 1997, A&A, 326, 632
Alencar, S. H. P., & Batalha, C. 2002, ApJ, 571, 378
Alencar, S. H. P., Johns-Krull, C. M., & Basri, G. 2001, AJ, 122, 3335
Alencar, S. H. P., Melo, C. H. F., Dullemond, C. P., Andersen, J., Batalha, C., Vaz, L. P. R., & Mathieu, R. D. 2003, A&A, 409, 1037
Alexander, R. D., Clarke, C. J., & Pringle, J. E. 2004a, MNRAS, 348, 879
———. 2004b, MNRAS, 354, 71
———. 2005, MNRAS, 358, 283
Armitage, P. J., Clarke, C. J., & Palla, F. 2003, MNRAS, 342, 1139
Armitage, P. J., Clarke, C. J., & Tout, C. A. 1999, MNRAS, 304, 425
Artymowicz, P., & Lubow, S. H. 1994, ApJ, 421, 651
Baraffe, I., Chabrier, G., Allard, F., & Hauschildt, P. H. 1998, A&A, 337, 403
Baraffe, I., Chabrier, G., Barman, T. S., Allard, F., & Hauschildt, P. H. 2003, A&A, 402, 701
Barsony, M., Koresko, C., & Matthews, K. 2003, ApJ, 591, 1064
Beckwith, S. V. W., Sargent, A. I., Chini, R. S., & Guesten, R. 1990, AJ, 99, 924
Bontemps, S., et al. 2001, A&A, 372, 173
Bouvier, J., & Appenzeller, I. 1992, A&AS, 92, 481
Brandner, W., & Zinnecker, H. 1997, A&A, 321, 220
Burrows, C. J., et al. 1996, ApJ, 473, 437
Butler, R. P., Vogt, S. S., Marcy, G. W., Fischer, D. A., Wright, J. T., Henry, G. W., Laughlin, G., & Lissauer, J. J. 2004, ApJ, 617, 580
Carpenter, J. M. 2001, AJ, 121, 2851
Clarke, C. J., Gendrin, A., & Sotomayor, M. 2001, MNRAS, 328, 485
Cohen, M., Walker, R. G., Barlow, M. B., & Deacon, J. R. 1992, AJ, 104, 1650
Cohen, M., Walker, R. G., Carter, B., Hammersley, P., Kidger, M., & Noguchi, K. 1999, AJ, 117, 1864
Cohen, M., Witteborn, F. C., Walker, R. G., Bregman, J. D., & Wooden, D. H. 1995, AJ, 110, 275
Cox, A., ed. 2000, Allen's Astrophysical Quantities (New York: AIP)
D'Alessio, P., et al. 2005, ApJ, 621, 461
de Geus, C. J., & Burton, W. B. 1991, A&A, 246, 559
Doppman, G. W., Jaffe, D. T., & White, R. J. 2003, AJ, 126, 3043
Duchêne, G., Ghez, A. M., McCabe, C., & Weinberger, A. J. 2003, ApJ, 592, 288
Duchêne, G., Monin, J.-L., Bouvier, J., & Ménard, F. 1999, A&A, 351, 954
Duquennoy, A., & Mayor, M. 1991, A&A, 248, 485
Dutrey, A., Guilloteau, S., Prato, L., Simon, M., Duvert, G., Schuster, K., & Ménard, F. 1998, A&A, 338, L63
Duvert, G., Guilloteau, S., Ménard, F., Simon, M., & Dutrey, A. 2000, A&A, 355, 165
Elias, J. H. 1978, ApJ, 224, 857
Folha, D. F. M., & Emerson, J. P. 2001, A&A, 365, 90
Ghez, A. M., Emerson, J. P., Graham, J. R., Meixner, M., & Skinner, C. J. 1994a, ApJ, 434, 707
Ghez, A. M., Klein, B. L., Morris, M., & Becklin, E. E. 1998, ApJ, 509, 678
Ghez, A. M., McCarthy, D. W., Weinberger, A. J., Neugebauer, J., & Matthews, K. 1994b, in ASP Conf. Ser. 56, Interacting Binary Stars, ed. A. W. Shafter (San Francisco: ASP), 221
Ghez, A. M., Neugebauer, G., Gorham, P. W., Haniff, C. A., Kulkarni, S. R., Matthews, K., Koresko, C., & Beckwith, S. V. W. 1991, AJ, 102, 2066
Ghez, A. M., Neugebauer, G., & Matthews, K. 1993, AJ, 106, 2005
Ghez, A. M., Weinberger, A. J., Neugebauer, G., Matthews, K., & McCarthy, D. W., Jr. 1995, AJ, 110, 753
Ghez, A. M., White, R. J., & Simon, M. 1997, ApJ, 490, 353
Girart, J. M., Curiel, S., Rodríguez, L. F., Honda, M., Cantó, J., Okamoto, Y. K., & Sako, S. 2004, AJ, 127, 2969
Greene, T. P., & Meyer, M. R. 1995, ApJ, 450, 233
Guilloteau, S., Dutrey, A., & Simon, M. 1999, A&A, 348, 570
Haisch, K. E., Jr., Lada, E. A., & Lada, C. J. 2001, ApJ, 553, L153
Hanner, M. S., Brooke, T. Y., & Tokunaga, A. T. 1998, ApJ, 502, 871
Hartigan, P., & Kenyon, S. J. 2003, ApJ, 583, 334
Hartigan, P., Strom, K. M., & Strom, S. E. 1994, ApJ, 427, 961
Hartmann, L. 1998, Accretion Processes in Star Formation (Cambridge: Cambridge Univ. Press)
Hartmann, L., Hewett, R., & Calvet, N. 1994, ApJ, 426, 669
Herbig, G. H., & Bell, K. R. 1988, Lick Obs. Bull., 1111, 1
Hollenbach, D., Johnstone, D., Lizano, S., & Shu, F. 1994, ApJ, 428, 654
Jensen, E. L. N., & Mathieu, R. D. 1997, AJ, 114, 301
Jones, B., & Puetter, R. C. 1993, Proc. SPIE, 1946, 610
Kenyon, S. J., Brown, D. I., Tout, C. A., & Berlind, P. 1998, AJ, 115, 2491
Kenyon, S. J., & Hartmann, L. 1995, ApJS, 101, 117
Kenyon, S. J., Yi, I., & Hartmann, L. 1996, ApJ, 462, 439
Koerner, D. W., Jensen, E. L. N., Cruz, K. L., Guild, T. B., & Gultekin, K. 2000, ApJ, 533, L37
Koresko, C. D. 2002, AJ, 124, 1082
Koresko, C. D., Herbst, T. M., & Leinert, Ch. 1997, ApJ, 480, 741
Lada, C. J. 1987, in IAU Symp. 115, Star Forming Regions, ed. M. Peimbert & J. Jugaku (Dordrecht: Reidel), 1
Leinert, Ch., Zinnecker, H., Weitzel, N., Christou, J., Ridgway, S. T., Jameson, R., Haas, M., & Lenzen, R. 1993, A&A, 278, 129
Littlefair, S. P., Naylor, T., Harries, T. J., Retter, A., & O'Toole, S. 2004, MNRAS, 347, 937
Lord, S. D. 1992, NASA Tech. Mem. 103957
Luhman, K. L., & Rieke, G. H. 1999, ApJ, 525, 440
Marchal, L., et al. 2003, in IAU Symp. 211, Brown Dwarfs, ed. E. L. Martin (San Francisco: ASP), 311
Marraco, H. G., & Rydgren, A. E. 1981, AJ, 86, 62
Martín, E. L. 1998, AJ, 115, 351
Mathieu, R. D., Stassun, K., Basri, G., Jensen, E. L. N., Johns-Krull, C. M., Valenti, J. A., & Hartmann, L. W. 1997, AJ, 113, 1841
Matsuyama, I., Johnstone, D., & Hartmann, L. 2003, ApJ, 582, 893
McCabe, C., Duchêne, G., & Ghez, A. M. 2002, ApJ, 575, 974
———. 2003, ApJ, 588, L113
Meyer, M. R., Calvet, N., & Hillenbrand, L. A. 1997, AJ, 114, 288
Muzerolle, J., Hartmann, L., & Calvet, N. 1998, AJ, 116, 2965
Myers, P. C., Fuller, G. A., Mathieu, R. D., Beichman, C. A., Benson, P. J., & Schild, R. E. 1987, ApJ, 319, 340
Natta, A., Meyer, M. R., & Beckwith, S. V. W. 2000, ApJ, 534, 838
Osterloh, M., & Beckwith, S. V. W. 1995, ApJ, 439, 288
Prato, L., & Simon, M. 1997, ApJ, 474, 455
Prato, L. A., Greene, T. P., & Simon, M. 2003, ApJ, 584, 853
Prato, L. A., et al. 2001, ApJ, 549, 590
Press, W. H., Teukolsky, S. A., Vetterling, W. T., & Flannery, B. P. 1992, Numerical Recipes in C: The Art of Scientific Computing (Cambridge: Cambridge Univ. Press)
Przygodda, F., van Boekel, R., Àbrahàm, P., Melnikov, S. Y., Waters, L. B. F. M., & Leinert, Ch. 2003, A&A, 412, L43
Quillen, A. C., Blackman, E. G., Frank, A., & Varnière, P. 2004, ApJ, 612, L137
Rayner, J. T., et al. 1993, Proc. SPIE, 1946, 490
Reipurth, B., & Zinnecker, H. 1993, A&A, 278, 81
Rieke, G. H., & Lebofsky, M. J. 1985, ApJ, 288, 618
Rydgren, A. E., Strom, S. E., & Strom, K. M. 1976, ApJS, 30, 307

Sargent, A. I., & Beckwith, S. V. W. 1991, ApJ, 382, L31
Shu, F. H., Adams, F. C., & Lizano, S. 1987, ARA&A, 25, 23
Shure, M. A., et al. 1994, Proc. SPIE, 2198, 614
Simon, M., Holfeltz, S. T., & Taff, L. G. 1996, ApJ, 469, 890
Simon, M., et al. 1995, ApJ, 443, 625
Skinner, S. L., Brown, A., & Walter, F. M. 1991, AJ, 102, 1742
Skrutskie, M. F., Dutkevitch, D., Strom, S. E., Edwards, S., Strom, K. M., & Shure, M. A. 1990, AJ, 99, 1187
Smith, K. W., Lewis, G. F., Bonnell, I. A., Bunclark, P. S., & Emerson, J. P. 1999, MNRAS, 304, 367
Stanke, T., & Zinnecker, H. 2000, in IAU Symp. 200, The Formation of Binary Stars, ed. B. Reipurth & H. Zinnecker (San Francisco: ASP), 38
Stapelfeldt, K. R., Krist, J. E., Menard, F., Bouvier, J., Padgett, D. L., & Burrows, C. J. 1998, ApJ, 502, L65
Stassun, K. G., Mathieu, R. D., Vrba, F. J., Mazeh, T., & Henden, A. 2001, AJ, 121, 1003
Strom, K. M., & Strom, S. E. 1994, ApJ, 424, 237
Strom, K. M., Strom, S. E., Edwards, S., Cabrit, S., & Skrutskie, M. F. 1989, AJ, 97, 1451
Takeuchi, T., Clarke, C. J., & Lin, D. N. C. 2005, ApJ, 627, 286
Telesco, C. M., et al. 2000, ApJ, 530, 329
Walter, F. M., Brown, A., Mathieu, R. D., Myers, P. C., & Vrba, F. J. 1988, AJ, 96, 297
White, R. J., & Ghez, A. M. 2001, ApJ, 556, 265
Wilking, B. A., Bontemps, S., Schuler, R. E., Greene, T. P., & André, P. 2001, ApJ, 551, 357
Wilking, B. A., Lada, C. J., & Young, E. T. 1989, ApJ, 340, 823
Wilking, B. A., Schwartz, R. D., & Blackwell, J. H. 1987, AJ, 94, 106
Woitas, J., Leinert, Ch., & Köhler, R. 2001, A&A, 376, 982
Wolk, S. J., & Walter, F. M. 1996, AJ, 111, 2066
Wood, K., Lada, C. J., Bjorkman, J. E., Kenyon, S. J., Whitney, B., & Wolff, M. J. 2002, ApJ, 567, 1183